Structural Visualization of HECT-type E3 ligase Ufd4 Accepting and Transferring Ubiquitin to Form K29/K48-branched Polyubiquitination

Xiangwei Wu[1,2,#] , Huasong Ai[1,#], Junxiong Mao[2,#] , Hongyi Cai[2], Lu-Jun Liang[2], Zebin Tong[2], Zhiheng Deng[2], Qingyun Zheng[1,*], Lei Liu[2,*], Man Pan[1,3,4,*]

[1]Institute of Translational Medicine, School of Pharmaceutical Sciences, School of Chemistry and Chemical Engineering, National Center for Translational Medicine (Shanghai), Shanghai Key Laboratory for Antibody-Drug Conjugates with Innovative Target, Shanghai Jiao Tong University, Shanghai, 200240, China.

[2]New Cornerstone Science Laboratory, Tsinghua-Peking Joint Center for Life Sciences, MOE Key Laboratory of Bioorganic Phosphorus Chemistry and Chemical Biology, Center for Synthetic and Systems Biology, Department of Chemistry, Tsinghua University, Beijing 100084, China.

[3]Center for Future Foods, Muyuan Laboratory, 110 Shangding, Road, Zhengzhou, Henan Province, 450016, China.

[4]Lead Contact.

[#]These authors contributed equally to this work: Xiangwei Wu, Huasong Ai, Junxiong Mao.

*To whom correspondence should be addressed: Man Pan, panman@sjtu.edu.cn; Lei Liu (lliu@mail.tsinghua.edu.cn); Qingyun Zheng, zheng_qy@sjtu.edu.cn

Abstract

The K29/K48-linked ubiquitination generated by the cooperative catalysis of E3 ligase Ufd4 and Ubr1 is an enhanced protein degradation signal, in which Ufd4 is responsible for introducing K29-linked ubiquitination to K48-linked ubiquitin chains to augment polyubiquitination. How HECT-E3 ligase Ufd4 mediates the ubiquitination event remains unclear. Here, we biochemically determine that Ufd4 preferentially catalyses K29-linked ubiquitination on K48-linked ubiquitin chains to generate K29/K48-branched ubiquitin chains and capture structural snapshots of Ub transfer cascades for Ufd4-mediated ubiquitination. The N-terminal ARM region and HECT domain C-lobe of Ufd4 are identified and characterized as key structural elements that together recruit K48-linked diUb and orient Lys29 of its proximal Ub to the active cysteine of Ufd4 for K29-linked branched ubiquitination. These structures not only provide mechanistic insights into the architecture of the Ufd4 complex but also provide structural visualization of branched ubiquitin chain formation by a HECT-type E3 ligase.

Introduction

Poly-ubiquitination, formed by attaching a glycine at the C-terminus of one ubiquitin (Ub) to an amino group (M1, K6, K11, K27, K29, K33, K48, K63) on the surface of another Ub, governs almost all cellular processes in eukaryotes[1]. The functional diversity of poly-ubiquitination arises from the variable conformations of Ub chains, which can encode different functional signals to regulate the stability, localization and interactions of proteins, ultimately determining the fate of their substrates, known as Ub code[2]. Among these Ub codes, K48-linked Ub chains represent the best studied, acting as degradation signals that target substrate proteins to the proteasome[3,4]. Importantly, there is increasing evidence indicating that K48-linked Ub chains can be simultaneously ubiquitinated on other Lys (K) sites, leading to the formation of branched Ub chains[5,6]. The assembly of branched Ub chain could edit the original conformation of K48-linked Ub chain, thereby altering the functional signal. For example, the E3 ligase anaphase-promoting complex (APC/C) and E2 enzyme UBE2S assemble K11 linkages on K48-linked Ub chains K11/K48-branched Ub chains. These branched chains greatly enhance the proteasomal recognition of kinase Nek2A, thereby promoting the degradation of cell cycle regulators in the early stages of mitosis[7]. Induced by IL-1β signalling, E3 ligases HUWE1 and TRAF6 collaborate to assemble K63/K48-branched Ub chains, ultimately enhancing the NF-κB signaling[8]. Given the fundamental role of branched Ub chains in biological regulation, understanding how branched Ub chains are precisely assembled is one of the central concerns and challenges in the field.

The K29/K48-heterotypic Ub chains, first discovered in the N-terminal degradation pathway, were shown to accelerate the degradation of N-end substrates[9]. These heterotypic Ub chains are catalysed by two different E3 ligases, Ubr1 and Ufd4, of which the E3 ligase Ufd4 is responsible for augmenting K48-linked Ub chains in a K29-linked-specific manner[9]. Notably, a recent study has observed that E3 ligase TRIP12, the human homologue of Ufd4, can promote small-molecule-induced degradation through K29/K48-branched Ub chains[10]. However, the mechanism through which Ufd4 introduces K29-linked Ub chains on K48-linked Ub chains to increase the processivity of polyubiquitination remains unknown.

HECT-type E3 ligases are unique in their catalytic mechanism. Recent structural studies of the E3-E2-ubiquitin complex[11,12], Ub-loaded E3 complex[13-15] or E3-Ub-substrate complex[16-18]have illustrated the conformational plasticity at different stages of the reaction cycle. However, the mechanism by which HECT-type E3 enzymes assemble specific branched Ub chains remains unexplored. In this work, we biochemically demonstrate that Ufd4 preferentially catalyses K29-linked

66 ubiquitination on K48-linked Ub chains, leading to the formation of K29/K48-branched Ub chains. By
67 employing the biomimetic chemical probes to trap the enzymatic intermediates during the formation
68 of branched Ub chains, we successfully determine the cryo-EM structures and reveal the mechanistic
69 details of how the substrate Ub chains are recognized by Ufd4 to assemble the branched Ub chains.
70 We also capture a structural snapshot of TRIP12 (the human homologue of Ufd4) transferring Ub onto
71 K48-linked diUb, confirming the evolutionary conservation of these enzymes. In summary, our work
72 showcases the inaugural structural visualization of HECT-E3 Ufd4 accepting and transferring Ub to
73 form K29/K48-branched polyubiquitination.

74

75 # Results

76 ## Ufd4 prefers to synthesize branched ubiquitin chains on K48-linked ubiquitin
77 chains

78 Previous studies have shown that Ubr1/Ufd4 together strengthened the ubiquitination and
79 degradation of the substrate (e.g., Scc1[9] and the O^{6me}G-DNA alkylguanine transferase Mgt1[19]) through
80 K29- and K48-linked polyubiquitin chains, in which Ufd4 has been proposed to be a potential E4-like
81 enzyme and act as a Ub chain elongation factor[20]. Accordingly, we began our study with the
82 reconstitution of Ufd4-mediated polyubiquitination reactions on the substrates of monoUb, K29-linked
83 diUb, or K48-linked diUb using the yeast Ub-activating enzyme (E1) Uba1, the Ub-conjugating
84 enzyme (E2) Ubc4, the HECT-type E3 ligase Ufd4, and wild-type (WT) Ub. Enhanced
85 polyubiquitination was observed on substrate K48-linked diUb compared to monoUb or K29-linked
86 diUb **(**Fig. 1a and Supplementary Fig. 1a-g**)**. The Ufd4 preference for K48-linked diUb was further
87 confirmed by activity assays on eight different chain-type diUb substrates (M1, K6, K11, K27, K29,
88 K33, K48 and K63 linkages) (Supplementary Fig. 1h). Moreover, Ufd4 ubiquitination assays on
89 different lengths of K48-linked Ub chains (tri-, tetra-, and penta-) suggested that the polyubiquitination
90 efficiency escalated with increasing chain length **(**Supplementary Fig. 1b**)**.

91 Next, the topology of the Ub chains generated by Ufd4 on K48-linked Ub substrates was
92 determined. First, our biochemical assay and mass spectrometric analysis revealed Ufd4 specifically
93 mediates K29-linked ubiquitination on monoubiquitinated substrate (here, monoubiquitinated degron

94 peptide, Supplementary Fig. 2a/b), in line with the previous results[21]. Meanwhile, the Ufd4-mediated
95 polyubiquitination activity on K48-linked Ub chain substrates was significantly reduced when Ub-
96 K29R mutant was used, supporting K29-linked ubiquitination on K48-linked Ub chain substrates
97 (Supplementary Fig. 1c-f). Middle-down MS analysis (termed Ub-clipping[22]) of the polyubiquitination
98 product (using K48-linked tetraUb as a representative substrate) revealed 21.9% of mono-Ub species
99 modified by double-glycine remnants, representing the generation of branched Ub chains. Additionally,
100 Ub fragments with double-glycine remnants on both K29 and K48 residues were detected in the
101 MS/MS spectrum (Fig. 1b-d, Supplementary Note). To further elucidate the ubiquitination site
102 preference of Ufd4, we performed ubiquitination assays using K48-linked diUb mutants with K29R
103 mutation in either the proximal or distal Ub as substrates. The biochemical results demonstrated that
104 mutants with proximal K29R mutations exhibited weak ubiquitination, whereas mutants with distal
105 K29R mutations remained efficiently ubiquitinated (Fig. 1e). Furthermore, the enzyme kinetics of
106 Ufd4 were determined individually for the aforementioned K48-linked diUb mutants and the results
107 revealed that the ubiquitination efficiency, as represented by k_{cat}/K_m (Supplementary Fig. 2c), is
108 approximately 5.2-fold higher at proximal K29 site (0.11 $\mu M^{-1}\cdot min^{-1}$) compared to distal K29 site
109 (0.021 $\mu M^{-1}\cdot min^{-1}$). We also prepared fluorescently labeled K48-linked triUb, with only one Ub
110 (proximal, middle, or distal) retaining the K29 site, while the K29 sites in the other two Ubs were
111 mutated to Arg (Supplementary Fig. 20) and then conducted Ufd4 ubiquitination experiments.
112 Branched ubiquitination was observed on K48-linked triUb with the K29-only site in either the
113 proximal or middle Ub. In contrast, under the same catalytic conditions, very weak ubiquitination
114 activity was detected on K48-linked triUb with the K29-only site in the distal Ub (Fig. 1f). Taken
115 together, these biochemical results suggest that Ufd4 preferentially catalyzes K29-linked Ub
116 conjugates on preassembled K48-linked Ub chains to form K29/K48-branched Ub chains.

117

118 Structural visualization of the K29/K48-branched ubiquitination by Ufd4

119 To investigate the molecular mechanism of how Ufd4 transfers its thioester-bound Ub to the
120 proximal K29 of the K48-linked diUb substrate, we covalently linked the catalytic residue of Ufd4
121 (C1450), the C-terminus of Ub and the proximal K29 of K48-linked diUb to form a stable complex to
122 mimic the corresponding transition state (Fig. 2). This complex was prepared in two steps: first, an
123 engineered K29/K48-branched triUb probe (named $triUb^{probe}$) was synthesized according to our
124 previously reported procedure[23-28], in which the proximal Ub of K48-linked diUb was chemically

125 ligated with the donor Ub (Fig. 2a, b and Supplementary Fig. 3c,d); then, triUb^{probe} was cross-linked
126 with Ufd4 in a catalytic residue (C1450)-dependent manner to form the designed stable complex mimic
127 (Supplementary Fig. 3a). This complex was subjected to single-particle cryo-EM analysis. A total of
128 5,332 micrographs were collected and processed to obtain a cryo-EM map at a global resolution of
129 3.31 Å (Supplementary Tab. 1 and Supplementary Fig. 21). The AlphaFold-predicted Ufd4 structure
130 (code: AF-P33202-F1) and the crystal Ub structure (PDB code: 1UBQ) were docked into the cryo-EM
131 maps with meticulous adjustments and iterative refinements to obtain the model of the complex
132 (Supplementary Fig. 4a, b).

133 The overall structure of Ufd4 with donor Ub conjugated on proximal K29 of K48-linked diUb
134 (named Ufd4-triUb$^{K29/K48}$ complex) resembles a closed ring shape, in which Ufd4 forms a clamp
135 sandwiching donor Ub and K48-linked diUb (Fig. 2d, e). The chemically stable linkage between donor
136 Ub C-terminus, Ufd4 active center, and acceptor Ub K29 mimics the native transition state
137 (Supplementary Fig. 3d). The N-terminal region of Ufd4 (1-163), which was reported to interact with
138 the proteasome[29], is invisible in our cryo-EM map, possibly due to intrinsic disorder. The visible Ufd4
139 scaffold consists of three regions: the armadillo-like (ARM) region (164-706) composed of multiple
140 repeating α-helices, the HECT domain that contains the N-lobe (1107-1360) and C-lobe (1367-1483),
141 and the multi-helix region (MHR) (707-1096) bridging the two regions mentioned above (Fig. 2c-e).
142 K48-linked diUb is bound by the C-lobe of the HECT domain and two helical repeats within the ARM
143 region, previously reported to recognize Ub-fusion proteins[30], which we term here as Ub-interacting
144 helical clusters (UIHC1, residues 263-301; UIHC2, residues 304-332) (Fig. 2c). Meanwhile, the donor
145 Ub is engaged by the C-lobe of the HECT domain, consistent with previous structural findings derived
146 from the HECT domain[13-15] or full-length UBR5[17].

147

148 Ufd4 binds the substrate (K48-linked diUb) through multidentate interfaces

149 The contact between Ufd4 and K48-linked diUb can be subdivided into interactions with proximal
150 Ub (named Ub$^{K48-prox}$) and distal Ub (named Ub$^{K48-dist}$) (Fig. 3a). Ub$^{K48-prox}$ is bound by UIHC2 and
151 the HECT C-lobe, where residues Thr315, Ile316 and His317 of UIHC2 are directed toward residue
152 Arg54 of Ub$^{K48-prox}$ (Fig. 3c and Supplementary Fig. 4f), and residues His1378 and His1433 of the
153 HECT domain C-lobe are pointed toward the hydrophilic surface formed by Ub$^{K48-prox}$ residues Pro19
154 and Ser20 (Fig. 3d and Supplementary Fig. 4g, 5c). This dual anchoring effect of UIHC2 and the

155 HECT C-lobe on $Ub^{K48\text{-}prox}$ orients its Lys29 side chain toward the active cysteine of Ufd4 (distance
156 between α-carbon atoms is 9.04 Å, Supplementary Fig. 5d). $Ub^{K48\text{-}dist}$ interacts with the Ufd4 UIHC1
157 and UIHC2 motifs through multiple hydrophobic interactions. Specifically, residues Tyr276, Ile277
158 and Asp278 of Ufd4 UIHC1 are located close to the Leu8 loop of $Ub^{K48\text{-}dist}$, and the side chain of
159 Phe313 of UIHC2 inserts into the hydrophobic I44 patch of $Ub^{K48\text{-}dist}$ formed by Ile44, His68, and
160 Val70 (Fig. 3b and Supplementary Fig. 4e, 5b), which often participate in recruiting Ub-binding
161 proteins[2]. Interestingly, these above interactions reshape K48-linked diUb to adopt an extended
162 conformation that differs from prior structures determined for either free K48-linked diUb or in
163 complex with various recognition proteins (e.g., Rpn13, SARS PLpro, MINDY1)[31-34] (Supplementary
164 Fig. 5a). Furthermore, the isolated Ufd4 ARM region (residues 164-706) binds to K48-linked diUb
165 with an affinity of 0.47 ± 0.15 μM, while no binding signal was detected in the case of monoUb
166 (Supplementary Fig. 5e). This indicates that the Ufd4 ARM region is a standalone Ub-binding domain
167 for K48-linked diUb, but not for monoUb.

168 The importance of the above key interacting surfaces was assessed by assaying the effects of
169 mutations in UICH1, UIHC2, and the HECT domain C-lobe of Ufd4. In Ufd4-mediated
170 polyubiquitination of K48-linked diUb, the Ufd4 UIHC1 triple mutant (Y276A/I277A/D278A, named
171 the YID mutant) slows down the activity by 25% (Fig. 3i). The Ufd4 UIHC2 triple mutant
172 (F313A/T315A/I316A, named FTI mutant) or single mutant H317A impairs the activity of Ufd4 by
173 90% or 70%, respectively (Fig. 3i). The HECT domain C-lobe H1433A mutant reduced activity by a
174 quarter (Fig. 3i). To gain further insight into the specific roles of these residues in branched
175 ubiquitination, we performed enzyme kinetic analysis on the FTI and H317A mutants (Supplementary
176 Fig. 2c, 6a-c), which exhibited the most pronounced defects in ubiquitination activity. Our results
177 showed that, compared to WT Ufd4, both FTI and H317A mutations had minimal impact on the
178 catalytic rate constant (k_{cat}), but led to a significant increase in the Michaelis constant (K_m). This
179 suggests that these residues play a crucial role in substrate binding, rather than in catalysis, which is
180 consistent with their location at the enzyme-substrate interface in the complex.

181

182 Interactions between the Ufd4 HECT domain C-lobe and the donor Ub

183 The donor Ub is primarily positioned by the C-terminal helix (residues 1462-1475) and the L2
184 loop (residues 1433-1445) of the C-lobe in the Ufd4 HECT domain (Fig. 3e and Supplementary Fig.

185 7a). We compared the structural organization between the C-lobe and donor Ub in our Ufd4-
186 triUb$^{K29/K48}$ complex with the canonical arrangement typified by the Ub-loaded NEDD4 HECT
187 domain structure (PDB code: 4BBN)[11] and E3-Ub-substrate complex (PDB code: 4LCD)[16]
188 **(**Supplementary Fig. 7b**)**. Structural alignment based on the C-lobe revealed that the donor Ub in our
189 structures displays a noticeable difference in orientation, exemplified by residue E34 of the donor Ub
190 in our structure flips 40.3° (compared to 4BBN) and 42.8° (compared to 4LCD) relative to C-lobe
191 residue Q1471 (measured by the α carbon atoms) and undergoes shifts of 15.66 Å (compared to 4BBN)
192 and 15.97 Å (compared to 4LCD), respectively.

193 In the C-terminal helix (1462-1475), residues R1468 and Q1471 are oriented towards the residues
194 L8 and T9 of donor Ub. Similarly, the corresponding C-terminal helix, such as that of NEDD4,
195 HUWE1, Rsp5 and UBR5, has also been observed to interact with donor Ub. Regarding the L2 loop
196 (1433-1445), it contains an insertion of five amino acids compared to the homologous loops, which
197 makes itself reach out and guide the rotation of donor Ub. Residues D1436, L1438, and E1442 are
198 proximal to the hydrophobic patch of donor Ub formed by residues I36 and L71 (Fig. 3f and
199 Supplementary Fig. 4h), and notably, residues D1436 and L1438 are located within this insertion.
200 Consistent with these structural observations, the Ufd4 R1468A mutant significantly impaired both
201 Ufd4~Ub thioester formation and ubiquitination of the K48-linked diUb substrate, while the Ufd4
202 E1442A mutant and the double mutant (D1436A/L1438A) exhibited varying reductions in Ufd4~Ub
203 thioester formation and substrate ubiquitination activity **(**Fig. 3j and Supplementary Fig. 7c, d**)**. The
204 above interaction positions the C-terminal thioester of the donor Ub proximal to the K29 side chain of
205 Ub$^{K48\text{-}prox}$, underlying the structural insight into Ufd4-catalyzed K29-linked branched ubiquitination
206 on K48-linked Ub chain (Fig. 3g, h).

207

208 Validation of key interactions between Ufd4 and K29/K48-branched triUb in vivo

209 To investigate the effect of the key interfaces observed in our structure, a 43-mer type-1 degron
210 peptide and a truncated substrate Scc1 (residues 268-384) were used in the Ufd4-mediated
211 polyubiquitination assay. The K48-linked Ub chains were first preassembled on these two substrates
212 using Ubr1 and its E2 enzyme Ubc2, and then further elongated by Ufd4 and its mutants. The
213 ubiquitination results showed that WT Ufd4 could further extend the polyubiquitin chain on the type-
214 1 degron peptide as well as the bona fide substrate Scc1 (residues 268-384), while the Ub chain

elongating activity was substantially reduced by the Ufd4 mutants FTI, R1468A, and H317A (Supplementary Fig. 8a, b, f).

To validate the structural mechanism in a physiological setting, a previously developed yeast growth assay was performed[19]. In *S. cerevisiae*, the ubiquitination level of Mgt1 is regulated by both Ufd4 and Ubr1, and its degradation leads to yeast death when exposed to the DNA alkylating agent MNNG[19]. We constructed a Ufd4-knockout yeast strain, and complementation with Ufd4 or its mutants altered Mgt1 ubiquitination levels, thus affecting the growth status of yeast (Supplementary Fig. 8c). When WT Ufd4 was introduced to complement the Ufd4-knockout yeast strain, exposure to the DNA-alkylating agent MNNG impaired the growth of the complemented strain. In contrast, under conditions without MNNG treatment, the growth phenotype of the Ufd4-knockout strain closely resembles that of the strain complemented with WT Ufd4 (Supplementary Fig. 8d). These results were consistent with previous in vivo degradation experiments showing that the Mgt1 level was affected by Ufd4[19]. Complementation with Ufd4 mutants (FTI, R1468A, or H317A) decelerated yeast death compared to WT Ufd4 with the addition of MNNG (Supplementary Fig. 8d). Moreover, the Ufd4-knockout strain was transformed with Myc-tagged Mgt1 and wild-type Ufd4 ($UFD4^{WT}$) or different mutants ($UFD4^{FTI}$, $UFD4^{H317A}$ and $UFD4^{R1468A}$), followed by a chase for 10 min to evaluate the decrease in Mgt1 protein levels mediated by different Ufd4 mutants. Complementation with $UFD4^{WT}$ was observed to promote the degradation of Mgt1, whereas complementing with mutated UFD4 reduced the degradation efficiency of Mgt1 (Supplementary Fig. 8e). These results support the correlation between the key interfaces of Ufd4 with K29/K48-branched triUb and their functional effects, highlighting the crucial role of these interactions in regulating Mgt1 degradation.

Conserved mechanism of K29/K48-branched ubiquitin chain formation by TRIP12

TRIP12 (the human homologue of Ufd4) has been discovered to be a positive regulator of PROTAC-induced neo-substrate degradation, facilitating this process by cooperating with the K48-linked Ub chain-specific CRL2 complex to form K29/K48-branched Ub chains[10]. This finding parallels Ufd4's preference for K48-linked Ub chains in generating K29/K48-branched Ub chains. We reconstructed the TRIP12-catalyzed ubiquitination using K48-linked diUb as a substrate and observed polyubiquitination of the substrate. Similar to Ufd4, TRIP12 exhibits the strongest ubiquitination

245 activity towards K48-linked diUb substrates among the eight different diUb linkage types
246 (Supplementary Fig. 9a, b). Middle-down MS analysis of the polyubiquitination product revealed 32.3%
247 of mono-Ub species modified by double-glycine remnants (Supplementary Fig. 9d), representing the
248 generation of branched Ub chains by TRIP12. Additionally, Ub fragments with double-glycine
249 remnants on both K29 and K48 residues were detected in the MS/MS spectrum (Supplementary Fig.
250 9e). Furthermore, we performed ubiquitination assays using K48-linked diUb mutants with K29R in
251 either the proximal or distal Ub as substrates. The biochemical results demonstrated that mutants with
252 proximal K29R mutations exhibited weak ubiquitination activity, whereas mutants with distal K29R
253 mutations remained efficiently ubiquitinated (Supplementary Fig. 9c), supporting the preference of
254 TRIP12 for the K29 site on proximal Ub to generate K29/K48-branched Ub chains. These results
255 suggest that TRIP12, like Ufd4, prefers K48-linked Ub chain substrates to assemble K29/K48-
256 branched Ub chains.

257 To visualize the catalytic assembly of K29/K48-branched Ub chains by TRIP12, triUb^{probe} was
258 also employed to obtain catalytic complex mimics, similar to the approach utilized for Ufd4. We
259 determined a cryo-EM structure of the TRIP12/triUb^{probe} complex at 3.63 Å, facilitated by the
260 AlphaFold2-predicted TRIP12 structure and the crystal structure of Ub as an initial template for
261 modelling (Supplementary Tab. 1 and Supplementary Fig. 22). For TRIP12, the armadillo-like (ARM)
262 region (442-1106), the multi-helix region (MHR) (1107-1584), and the catalytic HECT domain were
263 docked unambiguously (Fig. 4a, b). Among the three Ub units, the map was best defined for the
264 substrate K48-linked diUb. However, the map density for donor Ub was weak. The active Cys of
265 TRIP12 and the acceptor Ub residue K29 are located in the vicinity of 6.52 Å.

266 In the complex, TRIP12 binds to the substrate K48-linked diUb in a shape similar to that of the
267 Ufd4/triUb$^{K29/K48}$ complex, with the structural organization of the substrate remaining virtually
268 unchanged (Fig. 4c). The ARM region and the C-lobe of the HECT domain synergistically clamp the
269 K48-linked diUb, mirroring the recognition framework of Ufd4 (Supplementary Fig. 9f). The TRIP12
270 fragments corresponding to UICH1 and UICH2 interact with the distal Ub mainly through hydrophobic
271 interactions, and the interaction network closely resembles that observed in the Ufd4-distal Ub
272 interaction. Specifically, the L8 loop of distal Ub interacts with TRIP12 residues I533, I536, and F572.
273 Meanwhile, the I44 patch in distal Ub binds to residues F572 and I536 of TRIP12 (Fig. 4d). These key
274 residues of TRIP12 involved in interactions with the distal Ub are conserved from yeast to humans,
275 implying an important role for this interface in Ub recognition. For proximal Ub, as in the

276 Ufd4/triUb$^{K29/K48}$ complex, it engaged with UICH2 and the C-lobe. The proximal Ub residues R54 and
277 P19/S20, which also participate in binding with Ufd4 in the Ufd4/triUb$^{K29/K48}$ complex, interact with
278 residues S574/N576 in UICH2 and T1942/V1939 in the C-lobe of TRIP12, respectively (Fig. 4e, f).
279 Compared to the Ufd4/triUb $^{K29/K48}$ complex, the C-lobe of TRIP12 undergoes a slight shift, positioning
280 it closer to the proximal Ub (Fig. 4c). The cryo-EM density map indicated that E18 of the proximal
281 Ub establishes an ionic interaction with K1941 of the C-lobe (Fig. 4f); N25 in the proximal Ub inserts
282 into the hydrophobic cavity formed by M1957, V1960, and Y1962 on the C-lobe (Fig. 4g**)**; and the
283 backbone of G53 is adjacent to H1887 of the C-lobe, facilitating backbone hydrogen bonding
284 interaction (Fig. 4h**)**. Although these interactions were not observed in the Ufd4/triUb $^{K29/K48}$ complex
285 due to species differences, they did not reshape the proximal Ub orientation, which remains the same
286 as that observed in the Ufd4/triUb complex. To further explore the functional significance of these key
287 interactions, we generated TRIP12 mutants, including I533G/I536G/F572G,
288 V1939G/K1941A/T1942G, and M1957G/V1960G/Y1962G, and subjected them to ubiquitination
289 assays. The biochemical results showed that these mutations significantly reduced ubiquitination
290 activity (Supplementary Fig. 9g), emphasizing the crucial role of these interactions in TRIP12's
291 catalysis of K29/K48-branched Ub chain formation. Collectively, our biochemical and structural
292 analysis revealed a conserved enzymatic property and structural mechanism to form the K29/K48-
293 branched Ub chain by Ufd4 and TRIP12, providing insights into how TRIP12 accelerates PROTAC-
294 induced ubiquitination degradation of neo-substrates.

295

296 Cryo-EM structure of Ufd4 in complex with E2 enzyme Ubc4

297 To obtain a detailed understanding of the catalytic cascade of Ufd4, we determined the structure
298 of Ufd4 accepting Ub thioester from Ubc4. Thus, the active site of Ufd4, the C-terminus of Ub and the
299 active site of Ubc4 were chemically linked by a two-step method similar to that described above **(**Fig.
300 5**)**. An activity-based probe that relies on a chemically engineered Ubc4-Ub (named Ubc4-Ub^{probe}) was
301 first synthesized and then crosslinked with Ufd4 in an active center (C1450)-dependent manner to form
302 a stable complex mimic **(**Fig. 5a, b and Supplementary Fig. 3b, c**)**. The mimic was subjected to cryo-
303 EM analysis and provided three cryo-EM reconstructions, including a 3.52 Å map in which Ub and
304 Ufd4 (residue 1-706) were invisible, a 4.30 Å map with Ub and Ufd4 (residue 1-161) were invisible,
305 and a 6.39 Å map showing Ufd4 (residue, 1-706) was invisible while Ub was visible (Supplementary
306 Tab. 1 and Supplementary Fig. 23).

307 The primary distinction among the three maps above lies in the visibility of Ub and the N-terminal
308 region of Ufd4, and across all three maps, there is generally good overlap in the density of the Ufd4
309 HECT domain and Ubc4 (Supplementary Fig. 10a). Detailed structural analysis of Ufd4 with Ubc4
310 was then conducted by focusing on the highest resolution structure (3.52 Å), facilitated by the
311 AlphaFold-predicted Ufd4 structure (code: AF-P33202-F1) and the crystal structure of Ubc4 (PDB
312 code: 1QCQ) as a starting point for model building (Supplementary Fig. 4c, d). In this structure, the
313 catalytic cysteines of Ubc4 and Ufd4 are positioned closely, with an α-carbon distance of less than 8
314 Å, suggesting that this structure may represent an active trans-thioesterification state, though the Ub
315 is not visible.

316 Ubc4 is embraced by both the N-lobe and C-lobe of the Ufd4 HECT domain, exhibiting a similar
317 arrangement to the canonical HECT E3-E2 transthiolation complex, as exemplified by the NEDD4L-
318 Ubch5b-Ub complex[11] (Fig. 5c, Supplementary Fig. 10b). The contacts between the Ufd4 HECT
319 domain N-lobe and Ubc4 are contributed by multiple interfaces. The residue F63 of Ubc4, crucial for
320 determining the specificity of E2/E3 interaction, fits snugly into a hydrophobic groove formed by
321 L1262, L1266, I1269, L1284, Y1313, and other residues (Fig. 5e and Supplementary Fig. 4j),
322 reminiscent of how the homologous Phe residue in Ubch7 or Ubch5b binds to the parallel hydrophobic
323 surface of the E6AP or NEDD4L HECT domain. Indeed, the Ubc4 F63A mutant almost completely
324 diminished the trans-thioesterification activity (Fig. 5i). Three other interactions between N lobe and
325 Ubc4 are presented: the N-lobe residue D1292 and Ubc4 residue S3; the N-lobe residue S1281/S1283
326 and Ubc4 residue R6; the N-lobe residue Y1167 and Ubc4 residues P58, K64 and P65 (Fig. 5f, g and
327 Supplementary Fig. 4k, l). Mutations in these interface residues are deleterious for the formation of
328 E3~Ub thioester (Fig. 5i, j). The interaction between the Ufd4 HECT domain C-lobe and Ubc4
329 involves the pairing of C-lobe residue H1433 with Ubc4 residue H126 and the pairing of C-lobe residue
330 H1378 with Ubc4 residues V121, P122, and E123 (Fig. 5d and Supplementary Fig. 4i). The Ufd4
331 mutants H1433A and H1378A, as well as the Ubc4 mutant E123A and double mutant V121A/P122A,
332 all reduced the transfer of Ub from Ubc4 to Ufd4 (Fig. 5i, j).

333 In our structure, the HECT domain N- and C-lobes adopt the inverted T-conformation, as
334 observed in the NEDD4L and UBR5 transthiolation complex[11,17]. The interaction between N lobe
335 residues R1224, K1152, Y1181 and T1183, and residue I1417 on the C-lobe, plays a potential role in
336 stabilizing this conformation (Supplementary Fig. 11b). Indeed, when residue Ile1417 was mutated to
337 Gly1417, the E3~Ub thioester formation efficiency was reduced to ~20% compared to WT Ufd4 (Fig.

338 5j) and the branched ubiquitination was significantly impaired (Supplementary Fig. 10c). In
339 conclusion, Ubc4 and Ufd4 coordinate Ub transfer through a module similar to that described
340 previously[11,12].

341

342 **Transition model of Ufd4 from transthiolation to K29-linked Ub assembly**

343 The two structures we have resolved above correspond to the HECT E3 enzyme E2-to-E3
344 transthiolation state (Ufd4-Ubc4 complex structure) and the E3-to-substrate ubiquitination state (Ufd4-
345 triUb$^{K29/K48}$ complex structure). The similarities and differences between these two conformations
346 were analyzed to investigate the interdomain conformational changes of the HECT E3 enzyme in
347 different states.

348 First, we focused on the conformational differences of Ufd4 in complex with Ubc4 and triUb.
349 The structures of Ufd4-Ubc4 (which contains the ARM region) and Ufd4-triUb$^{K29/K48}$ were compared,
350 and the Ufd4 MHR (707-1096) and the N-lobe (1361-1107) superimpose well in these two structures
351 (Supplementary Fig. 11a). Notably, the ARM region (163-706) in the two structures undergoes
352 conformational changes; for instance, the Ufd4 residue Glu184 undergoes a 28.41 Å shift and a 14.8°
353 deflection relative to the residue His715. Next, we compared the structures of Ufd4-Ubc4 (the structure
354 at the highest resolution) and Ufd4-triUb$^{K29/K48}$ to identify the conformational changes in the HECT
355 domain of Ufd4 in different catalytic states. The structural organization of the HECT domain N-lobe
356 in these two structures remains unchanged during state transitions (Supplementary Fig. 11c), whereas,
357 similar to ubiquitination catalyzed by Rsp5 and UBR5, the C-lobe of the HECT domain adopts distinct
358 conformations during two different reaction states (transthiolation and substrate ubiquitination)
359 (Supplementary Fig. 11c). Finally, the Ufd4 C-lobe residues H1378 and H1433 were found to interact
360 with both Ubc4 and K48-linked diUb in the Ufd4 -Ubc4 and Ufd4-triUb$^{K29/K48}$ structures, respectively
361 (Fig. 3d, 5d), indicating that Ubc4 may need to disassociate beforehand and the C-lobe reorientates to
362 provide space for interactions with K48-linked diUb during the ubiquitination process.

363 Based on the structures of Ufd4-mediated Ub charging and ubiquitin transfer to the proximal
364 Lys29 site of K48-linked diUb, we proposed a functional model representing the whole catalytic
365 process of Ufd4. First, Ubc4~Ub is recruited by the HECT domain of Ufd4, followed by the loading
366 of Ub from Ubc4 and the discharge of Ubc4. Subsequently, the conformation of the ARM region and
367 C-lobe reorientates to jointly sandwich the K48-linked diUb substrate, which directs the proximal

368 Lys29 residue of K48-linked diUb toward Ufd4 catalytic Cys1450. Finally, the Ub thioester transfers
369 from Ufd4 catalytic Cys1450 to the proximal Lys29 of K48-linked diUb (Supplementary Fig. 11d).

370

371 # Discussion

372 Prior to proteasomal degradation, substrate proteins with destabilizing residues at the N-terminus
373 (termed as N-degrons) are often recognized by UBR family E3 ligases and ubiquitinated in a K48
374 linkage-specific manner[35]. This ubiquitination process on N-degron substrates can be further
375 augmented by another E3 ligase Ufd4 (a K29-linkage-specific HECT-type E3 ligase), leading to
376 accelerated substrate degradation[9,19]. The mechanism of a representative yeast Ubr1-catalyzed process,
377 including the initiation of N-degron ubiquitination and the K48 linkage-specific elongation step, was
378 recently elucidated by cryo-EM studies in our group[36]. Nonetheless, the mechanism through which
379 Ufd4 introduces K29-linked Ub chains on substrates to increase the processivity of polyubiquitination
380 remains unknown. Here, our biochemical and mass spectrometry experiments clarified key aspects of
381 the molecular mechanism of Ufd4, where Ufd4 preferentially catalyses branched ubiquitination on
382 K48-linked Ub chains, thereby elongating the Ub chain. To gain structural insight into this process,
383 we designed a mechanism-based chemical trapping strategy to study the Ufd4-specific ubiquitination
384 processes, specifically the transfer of Ub from the E2 enzyme to the E3 ligase, and subsequently from
385 the E3 ligase to the substrate. This strategy combined with cryo-EM provides valuable mechanistic
386 insights into how Ufd4 mediate the K29/K48-branched ubiquitination and enhances our understanding
387 of the catalytic mechanism underlying HECT E3 ligases. Meanwhile, our findings contribute to a
388 deeper understanding of linkage-specific polyubiquitin chain assembly by providing mechanistic
389 details specific to K29-linked ubiquitination, thereby complementing previous structural studies on
390 M1-, K11-, K48-, and K63-linked Ub chains[17,36-42]. Interestingly, the human homologue of Ufd4,
391 TRIP12, also preferentially assembles K29/K48-branched Ub chains through a conserved structural
392 mechanism, suggesting an evolutionarily conserved function across species.

393 A variety of structural elements responsible for acceptor Ub recognition have been identified
394 within the catalytic domains of E2 and E3 enzymes, which play a critical role in assembling Ub
395 chain[17,36-42]. For instance, a flexible loop in the E2 enzyme UBE2R2 is reshaped by the CRL RING
396 domain to precisely position the acceptor Ub within the catalytic site[42]. Likewise, a zinc finger motif

397 embedded in the RING2 domain of the RBR-type E3 ligase RNF216 engages the acceptor Ub, thereby
398 ensuring the selective generation of K63-linked Ub chains[40]. Despite these insights, the contribution
399 of non-catalytic regions in E2 and E3 enzymes to acceptor Ub recognition remains poorly understood.
400 A recent structural study on the HECT-type E3 ligase UBR5, which specifically assembles K48-linked
401 Ub chains, revealed that its N-terminal UBA domain binds an acceptor Ub, emphasizing the crucial
402 role of non-catalytic domains in dictating Ub chain assembly[17]. In this study, we found that the non-
403 catalytic N-terminal ARM domain of Ufd4/TRIP12 cooperates with the HECT catalytic domain to
404 precisely position the acceptor Ub, aligning its Lys29 toward the Ufd4/TRIP12 active site. Although
405 the N-terminal ARM domain may play a secondary role in this process, its involvement further
406 underscores the emerging concept that non-catalytic regions in Ub ligases contribute to Ub chain
407 assembly. Moving forward, it will be essential to investigate Ub chain assembly at the level of full-
408 length ubiquitination enzymes rather than focusing solely on their catalytic domains. Such studies will
409 provide deeper insights into the role of non-catalytic domains in acceptor Ub recognition.

410 Currently, structural studies on homotypic Ub chain assembly primarily focus on the formation
411 of diUb chains, where only the acceptor Ub unit needs to be recognized for chain elongation. In
412 contrast, a structural model for the generation of longer homotypic Ub chains has been established
413 mostly through the structural study of the UBE2K/RNF38 RING domain, which catalyzes the
414 formation of K48-linked triUb from K48-linked diUb[39]. In this model, only the acceptor (distal) Ub is
415 recognized, while the proximal Ub remains unbound. This raises the intriguing question of whether
416 branched Ub chain formation follows a similar recognition pattern. Specifically, in the case of
417 branched ubiquitination on a diUb substrate, does the recognition of the proximal Ub alone suffice to
418 initiate the branching process? Here, we found that for Ufd4/TRIP12, when K48-linked diUb serves
419 as the substrate, both the proximal and distal Ubs are recognized simultaneously. This suggests that,
420 at least in the case of Ufd4/TRIP12, unlike homotypic chain elongation, which relies solely on the
421 recognition of the distal Ub, the formation of branched Ub chains requires the recognition of multiple
422 Ubs. Building on this, we developed a working model for branched Ub chain assembly, highlighting
423 the key distinctions between homotypic and branched Ub chain formation. This observation raises the
424 question of whether the recognition of multiple Ubs for the position of the acceptor Ub is a common
425 feature among E3 ligases catalyzing branched ubiquitination, or if it is unique to Ufd4/TRIP12. We
426 anticipate that future structural studies on other branched Ub ligases will provide further insights.

427 # Methods

428 ## Cloning and plasmid construction

429 The plasmid encoding *S. cerevisiae Ufd4* gene was synthesized by GenScript (Nanjing, China), and its
430 codon was optimized for *S. cerevisiae* and *Escherichia coli* (*E. coli*) overexpression, respectively. For
431 overexpression by *S. cerevisiae*, the *Ufd4* gene was subcloned to the vector YEplac181 containing an
432 N-terminal DYKDDDDK (Flag) tag. For overexpression by *E. coli*, the gene was inserted between the
433 BamHI and EcoRI sites of the vector pGEX-4T-1 with an N-terminal GST tag followed by an HRV
434 3C protease cleavage site. The plasmid encoding human TRIP12 (442-1992) was also synthesized by
435 GenScript, and its codon was optimized for HEK293F overexpression, which was subcloned to the
436 vector pcDNA3.1 containing an N-terminal Flag tag. The DNA sequence encoding yeast (*S.*
437 *cerevisiae*) *Ubc4* was synthesized by GenScript and its codon was optimized for *E. coli*
438 overexpression. The gene was further cloned into the vector pET-28a with an N-terminal His tag
439 followed by an HRV 3C protease cleavage site. Different *Ufd4* and *Ubc4* mutants were constructed by
440 site-directed mutagenesis. The DNA sequences of wild-type Ub and Ub mutants including Ub-K6R,
441 Ub-K11R, Ub-K27R, Ub-K29R, Ub-K33R, Ub-K48R, Ub-K63R, Ub-G76C, Ub-K29R-G76C, Ub-
442 K29R/K48R, Ub-K29C/K48R, Ub-K29R/K63R, Ub-77D (a Ub variant with an additional amino acid
443 Asp at the C terminus), Ub-K29C/77D, M1-linked triUb mutant (distal and intermediate ubiquitin with
444 K29R mutation, proximal ubiquitin with G76C mutation) and Ub-MCQ (Ub variant with an additional
445 amino acid Cys between Met1 and Gln2) were constructed and cloned to the vector pET-22b by
446 GenScript. The plasmids containing *S. cerevisiae/*human *Uba1*, *S. cerevisiae Ubc2/*human *Ubch7*, *S.*
447 *cerevisiae Ubr1*, and the truncated *S. cerevisiae* genes *Scc1* (268–384; also known as MCD1) were the
448 same as previously used[12,36,43,44].

449

450 ## Protein expression and purification

451 Ufd4 used for cryo-EM sample and its mutants used in Ufd4-triUb$^{K29/K48}$ complex structure-related
452 ubiquitination assay were expressed in yeast and purified similarly to yeast Ubr1 as previously
453 described[36]. In brief, plasmids containing *Ufd4* and its mutants were transformed into yeast (BY4741)
454 cells. Single colonies were selected to grow in a synthetic medium with Leu defective resistance (SC,
455 −Leu) to an optical density at 600 nm (OD_{600}) of 2-3. The yeast cells were collected by centrifugation
456 at 5,000 × *g* and then fully resuspended with lysis buffer (50 mM HEPES, pH 7.5, 150 mM NaCl,
457 protease inhibitor cocktail (Roche), and 10% glycerol). The suspension liquid was frozen into small
458 balls and subsequently ground into a fine powder using a freezing grinder (SPEX Sample Prep 6870
459 Freezer/Mill). The powder was defrosted in ice water and centrifuged at 17,418 × *g* for 1 h. The
460 supernatant was loaded on the anti-Flag affinity resin (Thermo Fisher Scientific, A36803) and

461 incubated at 4°C for 2h. After washing adequately, 1 mg/mL Flag peptide dissolved in buffer (50 mM
462 HEPES, pH 7.5, 150 mM NaCl) was used to elute Flag-tagged Ufd4. Ufd4 was then purified by ion
463 exchange (Mono Q anion exchange column, GE Healthcare) with buffer A containing 50 mM HEPES,
464 pH 8.0 and buffer B containing 50 mM HEPES, pH 7.5, 1 M NaCl. Samples at indicated peaks were
465 concentrated and further purified using size exclusion chromatography (Superose 6 column, GE
466 Healthcare) with a buffer containing 50 mM HEPES, pH 7.5, and 150 mM NaCl. Finally, Ufd4 was
467 analyzed by SDS-PAGE (LabPAGE 4-12% 15 Wells, LABLEAD). Human TRIP12 (442-1992) was
468 expressed using HEK293F (Expi293F) cells and initially purified using anti-Flag affinity resin and
469 further purified using ion exchange (Mono Q) and exclusion chromatography (Superose 6 column),
470 similar to that of Ufd4.

471 The purification of Ubc2, Ubc4 and its variants were the same as previously[36] described. Briefly,
472 plasmids containing *Ubc4* and its variants were introduced into *E. coli* BL21(DE3) competent cells
473 and cultured in Luria Broth (LB) medium with 20 μg/mL kanamycin at 37°C to OD_{600} of 0.6. The cells
474 were cooled to 18°C and induced by 0.4 mM isopropylβ-d-1-thiogalactopyranoside (IPTG) for 16h.
475 The cells were centrifuged at 5,000 × *g* for 25 min at 4 °C and the precipitate was fully resuspended
476 with lysis buffer (50 mM HEPES, pH 7.5, 150 mM NaCl and 1 mM phenylmethyl sulfonyl fluoride
477 (PMSF). After lysed by sonication and 17,418 × *g* centrifugation, the supernatant was incubated with
478 Ni-NTA affinity column for 2 h at 4 °C. After washing with at least 10 column volumes of lysis buffer
479 (50 mM HEPES, pH 7.5, 150 mM NaCl, 20 mM imidazole), the proteins were eluted with a lysis buffer
480 containing 400 mM imidazole and further purified with size exclusion chromatography (Superdex 200
481 column, GE Healthcare) with a buffer containing 50 mM HEPES, pH 7.5, and 150 mM NaCl. The
482 expression of Ufd4 used in the Ufd4/Ubc4-Ub complex structure-related ubiquitination assay was
483 similar to Ubc4 as we described above. Differently, after lysis by sonication and high-speed
484 centrifugation, the supernatant was incubated with Glutathione beads for 2 h at 4°C. The protein was
485 eluted with a lysis buffer containing 30 mM Glutathione. The elution was incubated with HRV 3C
486 protease overnight to remove the GST tag and further purified as described above for yeast-expressed
487 Ufd4. Scc1(268–384) and Uba1 were obtained as we used before[36]. Wild-type (WT) Ub and Ub
488 mutants were purified as previously described[36].

489

490 **Yeast growth assay**

491 *S. cerevisiae* strain lacking *Ufd4* (*ΔUfd4*) was constructed by Thermo Fisher Scientific (item number:
492 YKL010C_34859). Ufd4 mutants (R1468A, FTI mutant, H317A) were constructed in the context of
493 the vector YEplac181, carrying the wild-type Ufd4.

494 Yeast strains lacking Ufd4 were plated in a rich (YPD) solid medium containing 2% agarose and 2%
495 glucose (w/v) and grown at 30°C for 2 days. Single colonies were selected to grow in a YPD liquid
496 medium at 30°C to mid-log-phase (OD_{600} of 0.4-0.8). Yeast cultures were centrifuged at 1,962 × *g* for
497 10 min and washed with double-distilled H_2O. Centrifuged again and resuspended with 1×TE buffer
498 (10 mM Tris-HCl, pH 8.0, 1 mM Ethylene Diamine Tetraacetic Acid (EDTA)). Repeated and
499 resuspended with 1×LiAc (100 mM LiAc, pH 7.5) and 0.5×TE buffer to obtain *ΔUfd4* competent yeast
500 cells and stored on ice for further use. WT Ufd4 and its mutants (R1468A, FTI mutant, H317A) were
501 transformed to *ΔUfd4* competent cells and plated in SD (−Leu) medium containing 2% agarose and 2%
502 glucose (w/v) at 30°C for 2 days.

503 Single colonies of the yeast strains mentioned above were selected to grow in SD (−Leu) medium
504 containing 2% glucose at 30°C overnight. Dilute with SD (−Leu) medium to OD_{600} of 0.4 and grow at
505 30°C until OD_{600} of 1.0. Add N-methyl-N'-nitro-N-nitrosoguanidine (MNNG) stock solution (50 mM
506 NaOAc, pH 5.0, 6 mM MNNG) to the final concentration of 60 μM and grow at 30°C for 1 h As
507 previously described[19]. Single colonies were spotted in serial fivefold dilution onto the SD (−Leu)
508 plates. The plates were grown at 30°C for 2 days before imaging.

509

510 **Preparation of Ub chains**

511 K29-linked chains were obtained with 0.2 μM Uba1, 4 μM Ubc4, 0.5 μM Ufd4, and 200 μM WT Ub
512 at 30°C in the reaction buffer (50 mM HEPES, pH 7.5, 150 mM NaCl, 10 mM $MgCl_2$ and 5 mM ATP).
513 K48-linked chains were obtained with 1 μM Uba1, 20 μM UBE2K and 800 μM WT Ub at 30°C in the
514 same reaction buffer. For K48-linked diUb variants, WT Ub was substituted with Ub mutants:
515 $diUb^{distal\text{-}K29}$(200 μM Ub-K29R/G76C and 200 μM Ub-K48R); $diUb^{prox\text{-}K29}$(200 μM Ub-G76C and 200
516 μM Ub-K29R/K48R); $diUb^{K29C}$(200 μM Ub-K29C/77D and 200 Ub-K48R). K48diUb was used for
517 kinetic assay (200 μM Ub-G76C and 200 μM Ub-K48R). The reactions were terminated by buffer (50
518 mM NaOAc, pH 4.5) and K29-linked and K48-linked chains were separated by ion exchange (Mono
519 S cation column, GE Healthcare) with buffer A containing 50 mM NaOAc, pH 4.5 and buffer B
520 containing 50 mM NaOAc, pH 4.5, 1 M NaCl. Samples at indicated peaks were collected and then
521 dialyzed into a buffer containing 50 mM HEPES, pH 7.5 and 150 mM NaCl, for further use.

522 For the triUb used in Figure 1f, E2 enzymes and deubiquitinating enzyme (YUH1) were combined to
523 prepare them (Supplementary Chemistry File 9). Briefly, Uba1(1μM), UBE2K or UBE2V/UBE2N (20
524 μM) and corresponding ubiquitin mutants (800 μM each) were incubated in the reaction buffer at 37°C
525 for 5-8 hours to generate the diUb variants. 7‰ trifluoroacetic acid (v/v) was added to terminate the
526 reaction, then the supernatant was collected and pH adjusted to 7.4, followed by the addition of YUH1
527 (0.8 μM) for overnight reaction. The diUb products were purified by ion exchange (Mono S cation

528 column, GE Healthcare) and dialyzed into a buffer containing 50 mM HEPES, pH 7.4 and 150 mM
529 NaCl, for further reaction. Next, the above diUb (400 μM), Ub-G76C or Ub-K29R-G76C (400 μM),
530 Uba1(1 μM), UBE2K or UBE2V/UBE2N (20 μM) were mixed and reacted at 37°C for 5-8 hours to
531 generate the triUb variants. and purified as above. M1/K6/K27/K29/K33/K48/K63-linked diUb were
532 obtained as we used before[44].

533

534 **Preparation of fluorescently labeled substrates**

535 Ub-MCQ, Ub-G76C, diUb$^{prox\text{-}K29}$, diUb$^{distal\text{-}K29}$, K48diUb used for the kinetic assay, triUb used in
536 Figure 1f were obtained as described above and were subjected to label. For the labeling reaction, 1.5
537 eq. of fluorescein-5-maleimide (Invitrogen, F150) was added to 2 mg Ub or Ub chain mutants, and the
538 mixtures were incubated at room temperature for 2 hours. The labeled proteins were purified with size-
539 exclusion chromatography (Superdex 200 column, GE Healthcare) with a buffer containing 50 mM
540 HEPES, pH 7.5, 150 mM NaCl.

541

542 ***In vitro* Ubiquitination assay**

543 *In vitro* ubiquitination assays were performed with 0.2 μM Uba1, 4 μM Ubc4 or Ubch7, 0.25 μM Ufd4
544 or TRIP12, 10 μM substrate Ub chains (M1/K6/K27/K29/K33/48/K63-linked diUb, K48-linked
545 diUb/triUb/tetraUb/pentaUb) or 2 μM fluorescently labeled substrates (fluorescent Ub-G76C, K48-
546 diUb, diUb$^{prox\text{-}K29}$, diUb$^{distal\text{-}K29}$ and M1/K48/K63-linked triUb) and 80 μM WT Ub or Ub-K29R at
547 30°C for Ufd4-related ubiquitination or 37°C for TRIP12-related ubiquitination in the reaction buffer
548 (50 mM HEPES, pH 7.5, 150 mM NaCl, 10 mM $MgCl_2$ and 5 mM ATP). For the ubiquitination assays
549 to validate key structural interfaces, the same concentrations of E1, E2, E3 enzyme, WT Ub, and
550 fluorescent diUb$^{prox\text{-}K29}$ were used.

551 To measure the ubiquitination activity on K48-linked substrate peptide and real N-end rule substrate,
552 another ubiquitination assays were performed with 0.2 μM Uba1, 4 μM Ubc2, 0.25 μM Ubr1, 4 μM
553 Ubc4, 0.25 μM Ufd4, 80 μM Ub, 5 μM (fluorescent degron, synthesized previously[36]) or 10 μM Scc1
554 (268–384) at 30°C with the same reaction buffer mentioned above.

555 These reactions were terminated by adding 4 × sodium dodecyl sulfate (SDS) sample buffer, and then
556 analyzed using SDS-PAGE and visualized by Coomassie Brilliant blue dye/fluorescence or visualized
557 by western blot using K29 linkage-specific antibodies[45] and K48 linkage-specific antibodies (Abcam,
558 ab190061).

559 **Kinetic measurement of Ub transfer on Ub and K48-linked diUb**

560 To measure the ubiquitination velocity between Ub and K48-linked diUb, a time-resolved kinetic
561 experiment was performed. *In vitro* ubiquitination assays were performed as described above, using
562 fluorescent Ub-G76C or K48diUb as the substrate. The reaction mixtures were sampled and terminated
563 by 4× SDS sample buffer at indicated time points (0, 1, 2, 5, 10, 15, 25, 45, 60 min), then analyzed
564 using SDS-PAGE and imaged by fluorescence. Data from three replicates were quantified by image
565 lab (Bio-Rad software) and time rate curves of ubiquitination were plotted.

566 **Transthiolation assay with fluorescently labeled Ub-MCQ**

567 Transthiolation assay consists of two operational steps. First, 0.1 μM Uba1, 5 μM Ubc4 or its variants,
568 10 μM fluorescently labeled Ub-MCQ were mixed at 30°C for 5 min in the reaction buffer (50 mM
569 HEPES, pH 7.5, 150 mM NaCl, 10 mM $MgCl_2$ and 5 mM ATP) to generate fluorescent ubiquitin-
570 loaded Ubc4 or its variants and then terminated with a final concentration of 250 mM EDTA (pH 7.4)
571 on ice. Next, the loaded Ubc4 or its variants was reacted with Ufd4 or its variants to the following final
572 concentrations: Ubc4 or its variants, 1.25 μM; fluorescent ubiquitin, 2.5 μM; Ufd4 or its variants, 0.5
573 μM and mixtures were sampled and terminated by 4× SDS sample buffer without Dithiothreitol (DTT)
574 at 30 seconds, then analyzed using SDS-PAGE and imaged by fluorescence (Bio-Rad).

575 **Mass spectrometry analysis of polyubiquitin chains**

576 To obtain polyubiquitin chains generated by Ufd4 or TRIP12 on K48-linked chains, *in vitro*
577 ubiquitination assay was performed as described above and K48-linked tetraUb was used as a
578 representative substrate. The reaction was quenched with 25 mM EDTA on ice. Then 5 μM engineered
579 viral protease Lb^{pro}* was added and incubated at 37°C overnight.

580 The identification and quantification of ubiquitin variants digested by Lb^{pro}* were described as
581 before[22]. In brief, diluted the reaction to 1 μM ubiquitin with a buffer (50 mM HEPES, pH 7.5, 150
582 mM NaCl). To perform high-mass protein analysis, samples were analyzed on a Q-TOF mass
583 spectrometer (SYNAPT G2-Si, Waters company) instrument. The raw native electrospray mass
584 spectra can be further deconvoluted by MaxEnt 1 (Waters) to generate a spectrum (relative intensity
585 versus mass). This spectrum allows a single species to transform all the charge-state peaks into a single
586 (zero-charge) peak. Microsoft Excel to further process the spectrum, and the intensities of un-
587 (8,451.65 Da), single- (8,565.69 Da), and double-modified (8,679.73 Da) ubiquitin were exported.

588 To identify the K29 site and K48 site double-modified ubiquitin, the reaction digested after Lb^{pro}* was
589 further treated with a low concentration of wild type alpha-lytic protease (WaLP) at 4°C for 2 h. To
590 analyze the specific linkage, a Thermo-Dionex Ultimate 3000 HPLC system was used and peptides

591 were separated by a 60 min gradient elution at a flow rate of 0.3 μL/min. This system allows direct
592 interface with the Thermo Orbitrap Fusion mass spectrometer. To identify peptide segments, the
593 MS/MS spectra obtained from each LC-MS/MS run were analyzed using the Proteome Discoverer
594 search algorithm (version 1.4), based on the target protein sequence. The search parameters were
595 configured as follows: the mass tolerance for precursor ions was set to 20 ppm for all MS scans, and
596 the mass tolerance for fragment ions was set to 0.02 Da for all acquired MS2 spectra. A fixed value
597 PSM validator was used to estimate the peptide false discovery rate (FDR), and a peptide-spectrum
598 match (PSM) was considered reliable if the q-value was below 1%.

599

600 **Isothermal titration calorimetry analysis**

601 All ITC experiments were performed using a MicroCal PEAQ-ITC (MicroCal) in a buffer (50 Mm
602 HEPES, 100 mM NaCl, pH 7.4) at 25 ℃. Purified Ufd4(164-706) fragment (28.5 μM) was titrated by
603 K48-linked diUb (460 μM) or monoUb (407 μM), respectively. Data analysis and fitting were
604 performed by MicroCal PEAQ-ITC Analysis Software.

605

606 **Cycloheximide Chase Analysis**

607 For the Mgt1 degradation assays, ΔUfd4 yeast strain (a gift from Wei Li, Guangzhou Medical
608 University) harboring the pRS313-Mgt1-6myc plasmid and the pRS316-Ufd4 plasmid or its variants
609 were grown in SD (−His/Ura) medium containing 2% glucose (w/v) at 30℃ to an OD_{600} of 0.7 and
610 then 68 μM MNNG was added to incubate for 40 min. Yeast cells were harvested by centrifugation
611 and washed two times with sterile water. Cycloheximide at a final concentration of 1 mg/ml was added
612 to the yeast cells and at each time point cells were collected and proteins were extracted as previously
613 described[21]. Briefly, the pelleted cells were resuspended in 0.2 M NaOH for 5min at 25℃, then
614 centrifuged to remove the supernatant and add 50ul loading buffer containing 8 M urea, 10% glycerol,
615 5% SDS, 1 mM EDTA, 100 mM DTT, 0.1% bromophenol blue and 0.2 M Tris-HCl, pH 6.8. The
616 samples were heated at 70 ° C for 8 min, followed by the supernatant after centrifugation was
617 subjected to SDS-PAGE. The Mgt1 and GAPDH were detected by immunoblotting analysis using an
618 anti-myc antibody (Cell Signaling Technology, 2272) and anti-GAPDH antibody (Proteintech, 60004-
619 1-Ig), respectively.

620

621 **Generation of the probe capturing the transition state of the K29 linkage assembly on K48-**
622 **linked diUb**

623 **Preparation of $Ub_{(1–76)}$-MesNa**

624 The $Ub_{(1–76)}$ hydrazine with a biotin tag at the N-terminus (1.0 equiv), prepared through protein
625 chemical synthesis as previously described[23], was dissolved in -15°C ligation buffer (2 mL, 100 mM
626 NaH_2PO_4, 6 M Gn-HCl, pH 2.3). Then, $NaNO_2$ (10 equiv) was added to the reaction, and the reaction
627 was stirred for 30 min at -15°C. After that, 2-mercaptoethanesulfonate (MesNa, 50 equiv) was added
628 to the reaction and the pH was slowly adjusted to 5.0-5.5. Next, the reaction reacted at room
629 temperature for 3-4 hours. Finally, ligation buffer was added to dilute the reaction before purification,
630 and the product was purified by semi-preparative HPLC using a Welch Ultimate XB-C4 column (21.2
631 × 150 mm, 5 μm particle size) and lyophilized.

632 **Preparation of K48 diUb-CAET-SAcm**

633 1mM $diUb^{K29C}$ with 40 mM (2-((2-chloroethyl)amino)ethane-1-(S-(Acetamidomethyl))thiol) were
634 incubated in alkylation buffer (6 M Gn-HCl, 0.2 M HEPES, 10 mM TCEP, pH=8.0-8.5) at 30°C for
635 overnight. The desired product was isolated by RP-HPLC and lyophilized.

636 **Preparation of K48 diUb-CAET-SH**

637 Lyophilized K48 diUb-CAET-SAcm (final concentration 1 mM) was dissolved in reaction buffer (6
638 M Gn-HCl, 0.2 M NaH_2PO_4 buffer, pH 7.4). Next, fresh $PdCl_2$ (15 equiv) was added to the reaction
639 and the reaction was incubated at 30°C for 2-3 h. Finally, the reaction was quenched by adding DTT
640 at a final concentration of 1 mM, and then the product was purified by semi-preparative HPLC and
641 lyophilized.

642 **Preparation of K29/48 branched triUb-SH**

643 Lyophilized K48 diUb-CAET-SH (1.0 equiv.) was dissolved in reaction buffer (6 M Gn-HCl, 100 mM
644 NaH_2PO_4, Ph 7.4) to a final concentration of 1 mM. Next, 4-mercaptophenylacetic acid (MPAA, 50
645 equiv.) and $Ub_{(1–76)}$-MesNa(1.5 equiv.) were added to the reaction buffer and the pH was adjusted to
646 6.5. Then, the reaction mixture was stirred at room temperature overnight, and the product was purified
647 by semi-preparative HPLC and lyophilized.

648 **Preparation of K29/48 branched triUb probe**

649 Lyophilized K29/48-triUb (1.0 equiv.) was dissolved in 1 mL buffer containing 6 M guanidinium
650 chloride, 0.1 M NaH_2PO_4 buffer, pH 7.4 at a final concentration of 2 mg/mL. Then, 2,2′-Dipyridyl
651 disulfide (AT_2, 25 equiv.) was added to the buffer and the reaction mixture was stirred at room
652 temperature for 2 h. Finally, the desired probe was purified and refolded with a Superdex75 column
653 (GE Healthcare) pre-equilibrated with 50 mM HEPES, pH 8.0, 150 mM NaCl.

654

655 **Generation of the probe capturing the transition state of the Ufd4-Ubc4 transthiolation**

656 **Preparation of $Ub_{(1–75)}$-MesNa**

657 The $Ub_{(1–75)}$ hydrazine was prepared from Ub-G76C as previously described[46] and was dissolved in -
658 15°C ligation buffer (2 mL, 100 mM NaH_2PO_4, 6 M Gn-HCl, pH 2.3). $NaNO_2$(10 equiv) and 2-
659 mercaptoethanesulfonate (MesNa, 50equiv) were then added to the reaction sequentially, as in the
660 preparation of $Ub_{(1–76)}$-MesNa. Finally, ligation buffer was added to dilute the reaction before
661 purification, and semi-preparative HPLC and lyophilized purified the product.

662 **Preparation of Ubc4-CAET-SAcm**

663 1mM Ubc4 mutant with only one Cys at C86 (Ubc4 C only) with 40 mM (2-((2-
664 chloroethyl)amino)ethane-1-(S-(Acetamidomethyl))thiol) were incubated in alkylation buffer (6 M
665 Gn-HCl, 0.2 M HEPES, 10 mM TCEP, pH = 8.0-8.5) at 30°C for overnight. The desired product was
666 isolated by RP-HPLC and lyophilized.

667 **Preparation of Ubc4-CAET-SH**

668 Lyophilized Ubc4-CAET-SAcm (final concentration 1 mM) was dissolved in reaction buffer (6 M
669 Gn·HCl, 0.2 M NaH_2PO_4 buffer, pH 7.4). Next, fresh $PdCl_2$ (15 equiv) was added to the reaction and
670 the reaction was incubated at 37°C for 2-3h. Finally, the reaction was quenched by adding DTT at a
671 final concentration of 1 mM, and then the product was purified by semi-preparative HPLC and
672 lyophilized.

673 **Preparation of Ubc4-Ub-SH**

674 Lyophilized Ubc4-CAET-SH (1.0 equiv.) was dissolved in reaction buffer (6 M Gn-HCl, 100 mM
675 NaH_2PO_4, Ph 7.4) to a final concentration of 1 mM. Next, 4-mercaptophenylacetic acid (MPAA, 50
676 equiv.) and $Ub_{(1–75)}$-MesNa(1.5 equiv.) were added to the reaction buffer and the pH was adjusted to
677 6.5. Then, the reaction mixture was stirred at room temperature overnight, and the product Ubc4-Ub
678 was purified by semi-preparative HPLC and lyophilized.

679 **Preparation of Ubc4-Ub probe**

680 Lyophilized Ubc4-Ub (1.0 equiv.) was dissolved in 1 mL buffer containing 6 M guanidinium chloride,
681 0.1 M NaH_2PO_4 buffer, pH 7.4 at a final concentration of 1.5 mg/mL. Then, 25 equiv. AT_2 (2,2′-
682 Dipyridyl disulfide) was added to the buffer and the reaction mixture was stirred at room temperature

683 for 2 h. Finally, the desired product, Ubc4-Ub probe, was purified and refolded with Superdex75
684 column pre-equilibrated with 50 mM HEPES, pH 8.0, 150 mM NaCl.

685 **Sample preparation for single-particle cryo-EM**

686 1.5 or 4.0 equiv K29/48 branched triUb probe, or Ubc4-Ub probe was mixed with Ufd4 (0.6 mg/mL)
687 and incubated at 30°C in a water bath for 30 min. For TRIP12, 4.0 equiv K29/48 branched triUb probe
688 was mixed with TRIP12 (0.6 mg/mL) and incubated at 25°C for 2 min. Prior to grid freezing using a
689 Vitrobot mark IV (Thermo Fisher Scientific) running at 8°C and 100% humidity, 0.0001% fluorinated
690 octyl maltoside (final concentration) was added to the samples. A volume of 3.5 µL sample was applied
691 to glow-discharged Quantifoil Au 1.2/1.3 grids for 1 min and blotted for 1 s or 3 s, then immersed in
692 liquid ethane to freeze.

693

694 **Cryo-EM Data collection and image processing**

695 Cryo-EM micrographs were collected on a 300 kV Titan Krios microscope equipped with a Gatan K3
696 or Falcon 4 direct electron detector camera. Images were recorded using AutoEmation 2.0 at a pixel
697 size of 1.074 or 0.808 Å with a total of 50 electrons over 32 frames. The defocus was set in a range of
698 -1.5 µm to -2.0 µm. MotionCor2 (v. 1.2.6)[47] and Gctf (v. 1.88)[48] were used for motion correction and
699 CTF parameter estimation. All the data were processed on RELION (v. 3.1)[49] for particle picking, 2D
700 classification, 3D classification, mask generation, refinement, postprocessing, and polishing. The
701 detailed processing workflow can be found in Supplementary Fig. 21-23.

702

703 **Model building, refinement and validation**

704 The cryo-EM maps of the Ufd4-triUb$^{K29/K48}$ complex, TRIP12-triUb$^{K29/K48}$ complex, and Ufd4/Ubc4-
705 Ub complex sharped at different B-factors were used for model building. The AlphaFold predicted
706 Ufd4 structure (code: AF-P33202-F1), AlphaFold predicted TRIP12 structure (code: AF-Q14669-F1-
707 v4), ubiquitin (PDB code: 1UBQ) and Ubc4 (PDB code: 1QCQ) were fitted into the cryo-EM maps
708 with rigid-body refinement in UCSF ChimeraX (v. 1.2.5)[50]. The individual models were merged into
709 one molecule in WinCoot (V. 0.8.2)[51]. Real-space refinement in Phenxi (1.19.2)[52] was subsequently
710 carried out with secondary structure constraints and/or geometry restraints. Further iterative manual
711 visualization and adjustment were conducted to give the final models. The statistics model building,
712 refinement and validation were summarized in Extended Data Table S1. Structural analysis and figure
713 layout were prepared in ChimeraX (v. 1.2.5).

Data Availability

The cryo-EM maps and corresponding atomic coordinates generated in this study have been deposited in the Electron Microscopy Data Bank (EMDB) and Protein Data Bank (PDB) under accession codes EMD-35929 [https://www.ebi.ac.uk/emdb/EMD-35929], 8J1P (Ufd4-triUb$^{K29/48}$) [https://www.rcsb.org/structure/8J1P]; EMD-35931 [https://www.ebi.ac.uk/emdb/ EMD-35931], 8J1R (Ufd4 in complex with Ubc4-Ub) [https://www.rcsb.org/structure/8J1R]; EMD-62292 [https://www.ebi.ac.uk/emdb/EMD-62292], 9KEN (TRIP12-triUb$^{K29/48}$) [https://www.rcsb.org/structure/9KEN]. The MS/MS data generated in this study have been deposited to the ProteomeXchange Consortium via the PRIDE partner repository with the dataset identifier PXD062799 [https://www.ebi.ac.uk/pride/archive/projects/PXD062799]. Data for mass spectrometry characterization of semisynthetic proteins generated in this study are provided in Supplementary Fig.12-19. The atomic model of ubiquitin, Ubc4, Ub-loaded NEDD4 HECT domain, and E3-Ub-substrate complex are available under PDB accession codes 1UBQ [http://doi.org/10.2210/pdb1UBQ/pdb], 1QCQ [http://doi.org/10.2210/pdb1QCQ/pdb], 4BBN [http://doi.org/10.2210/pdb4BBN/pdb], and 4LCD [http://doi.org/10.2210/pdb4LCD/pdb]. The predicted atomic model of Ufd4 and TRIP12 are available in the AlphaFold Protein Structure Database under accession codes AF-P33202-F1 [https://alphafold.ebi.ac.uk/entry/P33202]and AF-Q14669-F1-v4 [https://alphafold.ebi.ac.uk/entry/ Q14669]. Newly created materials from this study may be requested from the corresponding authors. Source data are provided with this paper.

References

1. Komander, D. & Rape, M. The Ubiquitin Code. *Annual review of biochemistry* **81**, 203-229 (2012).
2. Husnjak, K. & Dikic, I. Ubiquitin-Binding Proteins: Decoders of Ubiquitin-Mediated Cellular Functions. *Annual review of biochemistry* **81**, 291-322 (2012).
3. Ding, Z. et al. Structural Snapshots of 26S Proteasome Reveal Tetraubiquitin-Induced Conformations. *Molecular Cell* **73**, 1150-1161.e6 (2019).
4. de la Peña, A.H., Goodall, E.A., Gates, S.N., Lander, G.C. & Martin, A. Substrate-engaged 26S proteasome structures reveal mechanisms for ATP-hydrolysis–driven translocation. *Science* **362**, eaav0725 (2018).
5. Kolla, S., Ye, M., Mark, K.G. & Rapé, M. Assembly and function of branched ubiquitin chains. *Trends in Biochemical Sciences* **47**, 759-771 (2022).
6. French, M.E., Koehler, C.F. & Hunter, T. Emerging functions of branched ubiquitin chains. *Cell Discovery* **7**, 6 (2021).

7. Meyer, H.-J. & Rape, M. Enhanced Protein Degradation by Branched Ubiquitin Chains. *Cell* **157**, 910-921 (2014).
8. Ohtake, F., Saeki, Y., Ishido, S., Kanno, J. & Tanaka, K. The K48-K63 branched ubiquitin chain regulates NF-κB signaling. *Molecular Cell* **64**, 251-266 (2016).
9. Hwang, C.-S., Shemorry, A., Auerbach, D. & Varshavsky, A. The N-end rule pathway is mediated by a complex of the RING-type Ubr1 and HECT-type Ufd4 ubiquitin ligases. *Nature Cell Biology* **12**, 1177-1185 (2010).
10. Kaiho-Soma, A. et al. TRIP12 promotes small-molecule-induced degradation through K29/K48-branched ubiquitin chains. *Molecular Cell* **81**, 1411-1424.e7 (2021).
11. Kamadurai, H.B. et al. Insights into ubiquitin transfer cascades from a structure of a UbcH5B∼ubiquitin-HECTNEDD4L complex. *Molecular Cell* **36**, 1095-1102 (2009).
12. Huang, L. et al. Structure of an E6AP-UbcH7 Complex: Insights into Ubiquitination by the E2-E3 Enzyme Cascade. *Science* **286**, 1321-1326 (1999).
13. Maspero, E. et al. Structure of a ubiquitin-loaded HECT ligase reveals the molecular basis for catalytic priming. *Nature Structural & Molecular Biology* **20**, 696-701 (2013).
14. Jäckl, M. et al. β-Sheet Augmentation Is a Conserved Mechanism of Priming HECT E3 Ligases for Ubiquitin Ligation. *Journal of Molecular Biology* **430**, 3218-3233 (2018).
15. Nair, R.M. et al. Reconstitution and Structural Analysis of a HECT Ligase-Ubiquitin Complex via an Activity-Based Probe. *ACS Chemical Biology* **16**, 1615-1621 (2021).
16. Kamadurai, H.B. et al. Mechanism of ubiquitin ligation and lysine prioritization by a HECT E3. *eLife* **2**, e00828-1126 (2013).
17. Hehl, L.A. et al. Structural snapshots along K48-linked ubiquitin chain formation by the HECT E3 UBR5. *Nature Chemical Biology* **20**, 190-200 (2024).
18. Lorenz, S. Structural mechanisms of HECT-type ubiquitin ligases. *Biological chemistry* **399**, 127-145 (2018).
19. Hwang, C.-S., Shemorry, A. & Varshavsky, A. Two proteolytic pathways regulate DNA repair by cotargeting the Mgt1 alkylguanine transferase. *Proceedings of the National Academy of Sciences* **106**, 2142-2147 (2009).
20. Metzger, M.B. & Weissman, A.M. Working on a chain: E3s ganging up for ubiquitylation. *Nature Cell Biology* **12**, 1124-1126 (2010).
21. Liu, C., Liu, W., Ye, Y. & Li, W. Ufd2p synthesizes branched ubiquitin chains to promote the degradation of substrates modified with atypical chains. *Nature Communications* **8**, 14274 (2017).
22. Swatek, K.N. et al. Insights into ubiquitin chain architecture using Ub-clipping. *Nature* **572**, 533-537 (2019).
23. Zheng, Q. et al. An E1-Catalyzed Chemoenzymatic Strategy to Isopeptide-N-Ethylated Deubiquitylase-Resistant Ubiquitin Probes. *Angewandte Chemie International Edition* **59**, 13496-13501 (2020).
24. Zheng, Q. et al. A bifunctional molecule-assisted synthesis of mimics for use in probing the ubiquitination system. *Nature Protocols* **18**, 530-554 (2023).
25. Ai, H. et al. Synthetic E2-Ub-nucleosome conjugates for studying nucleosome ubiquitination. *Chem* **9**, 1221-1240 (2023).
26. Ai, H. et al. Mechanism of nucleosomal H2A K13/15 monoubiquitination and adjacent dual monoubiquitination by RNF168. *Nature Chemical Biology* (2024).
27. Shi, Q. et al. Promotion of RNF168-Mediated Nucleosomal H2A Ubiquitylation by Structurally Defined K63-Polyubiquitylated Linker Histone H1. *Angewandte Chemie International Edition* **64**, e202413651 (2025).

28. Dong, S. et al. Recent advances in chemical protein synthesis: method developments and biological applications. *Science China Chemistry* **67**, 1060-1096 (2024).
29. Xie, Y. & Varshavsky, A. UFD4 lacking the proteasome-binding region catalyses ubiquitination but is impaired in proteolysis. *Nature Cell Biology* **4**, 1003-1007 (2002).
30. Ju, D., Wang, X., Xu, H. & Xie, Y. The armadillo repeats of the Ufd4 ubiquitin ligase recognize ubiquitin-fusion proteins. *FEBS Letters* **581**, 265-270 (2007).
31. Liu, Z. et al. Structural basis for the recognition of K48-linked Ub chain by proteasomal receptor Rpn13. *Cell Discovery* **5**, 19 (2019).
32. Békés, M. et al. Recognition of Lys48-Linked Di-ubiquitin and Deubiquitinating Activities of the SARS Coronavirus Papain-like Protease. *Molecular Cell* **62**, 572-585 (2016).
33. Abdul Rehman, S.A. et al. Mechanism of activation and regulation of deubiquitinase activity in MINDY1 and MINDY2. *Molecular Cell* **81**, 4176-4190.e6 (2021).
34. Kristariyanto, Y.A., Abdul Rehman, S.A., Weidlich, S., Knebel, A. & Kulathu, Y. A single MIU motif of MINDY- 1 recognizes K48- linked polyubiquitin chains. *EMBO reports* **18**, 392-402-402 (2017).
35. Tasaki, T., Sriram, S.M., Park, K.S. & Kwon, Y.T. The N-End Rule Pathway. *Annual review of biochemistry* **81**, 261-289 (2012).
36. Pan, M. et al. Structural insights into Ubr1-mediated N-degron polyubiquitination. *Nature* **600**, 334-338 (2021).
37. Stieglitz, B. et al. Structural basis for ligase-specific conjugation of linear ubiquitin chains by HOIP. *Nature* **503**, 422-426 (2013).
38. Brown, N.G. et al. Dual RING E3 Architectures Regulate Multiubiquitination and Ubiquitin Chain Elongation by APC/C. *Cell* **165**, 1440-1453 (2016).
39. Nakasone, M.A. et al. Structure of UBE2K–Ub/E3/polyUb reveals mechanisms of K48-linked Ub chain extension. *Nature Chemical Biology* **18**, 422-431 (2022).
40. Cotton, T.R. et al. Structural basis of K63-ubiquitin chain formation by the Gordon-Holmes syndrome RBR E3 ubiquitin ligase RNF216. *Molecular Cell* **82**, 598-615.e8 (2022).
41. Branigan, E., Plechanovová, A., Jaffray, E.G., Naismith, J.H. & Hay, R.T. Structural basis for the RING-catalyzed synthesis of K63-linked ubiquitin chains. *Nature Structural & Molecular Biology* **22**, 597-602 (2015).
42. Liwocha, J. et al. Mechanism of millisecond Lys48-linked poly-ubiquitin chain formation by cullin-RING ligases. *Nature Structural & Molecular Biology* **31**, 378-389 (2024).
43. Ye, Y. et al. Semi-synthesis of K27-linked-mixed-triubiquitin chains through a combination of enzymatic reaction with CAACU strategy. *Tetrahedron Letters* **71**, 153000 (2021).
44. Wu, X. et al. Structure-guided engineering enables E3 ligase-free and versatile protein ubiquitination via UBE2E1. *Nature Communications* **15**, 1266 (2024).
45. Yu, Y. et al. K29-linked ubiquitin signaling regulates proteotoxic stress response and cell cycle. *Nature Chemical Biology* **17**, 896-905 (2021).
46. Chu, G.-C. et al. Efficient semi-synthesis of ubiquitin-7-amino-4-methylcoumarin. *Tetrahedron* **74**, 3931-3935 (2018).
47. Zheng, S.Q. et al. MotionCor2: anisotropic correction of beam-induced motion for improved cryo-electron microscopy. *Nature Methods* **14**, 331-332 (2017).
48. Mindell, J.A. & Grigorieff, N. Accurate determination of local defocus and specimen tilt in electron microscopy. *Journal of Structural Biology* **142**, 334-347 (2003).
49. Zivanov, J. et al. New tools for automated high-resolution cryo-EM structure determination in RELION-3. *eLife* **7**, e42166 (2018).
50. Pettersen, E.F. et al. UCSF ChimeraX: Structure visualization for researchers, educators, and developers. *Protein Science* **30**, 70-82 (2021).

51. Emsley, P. & Cowtan, K. Coot: model-building tools for molecular graphics. *Acta Crystallographica Section D* **60**, 2126-2132 (2004).
52. Adams, P.D. et al. PHENIX: a comprehensive Python-based system for macromolecular structure solution. *Acta Crystallographica Section D* **66**, 213-221 (2010).

Acknowledgments

We thank the National Natural Science Foundation of China (92253302, T2488301, 22137005, and 22227810 to L. L.; 22277073 and 92253302 to M. P.), National Key R&D Program of China (2022YFC3401500 to L. L.; 2023YFA0915300 to M. P.; 22407085 for Q.Z.), New Cornerstone Science Foundation (to L. L.). Shanghai Rising-Star Program (22QA1404900 to M. P.), Shanghai Pilot Program for Basic Research - Shanghai Jiao Tong University (21TQ1400224 to M. P.), Foundation of Muyuan Laboratory (118602240 to M. P.). Fundamental Research Funds for the Central University (to M. P.). Shanghai Jiao Tong University 2030 Initiative (WH510363003/003 to M. P., WH510363002/009 to Q. Z.), Shanghai Frontiers Science Center of Drug Target Identification and Delivery (ZXWH2170101 to H. A.), Chenguang Program of Shanghai Education Development Foundation (25Z520401224 to Q.Z.). We acknowledge the Tsinghua University Branch of China National Center for Protein Sciences (Beijing) for cryo-EM screening and data collection in 200 kV Arctica Tecnai microscopy and 300 kV Titan Krios microscopy. We also thank Shuimu BioSciences for Cryo-EM facility access and technical support during image acquisition.

Author Contributions Statement

Conceptualization: X. W., H. A., J. M., Q. Z., L. Liu., and M. P. Design of experiments: X. W., H. A., J. M., Q. Z., L. Liu., and M. P. Synthesis of E2-to-E3 transthiolation intermediate mimics: J. M. Synthesis of E3-to-substrate ubiquitination intermediate mimics: X. W. and J. M. Cryo-EM sample preparation: J. M., X. W., and H. A. Structural determination of cryo-EM structures: H. A. and X.W. Structural modeling of the native transition states and chemically stable mimics: Z. D. Synthesis of fluorescently labelled K48-linked diUb and Ub: J. M., and X.W. Cloning and purification of E1, Ufd4, Ubc4, and all their mutants: J. M., X.W., H. C., L. Liang., and Z. T. Ufd4-related in vitro enzymatic assays and yeast assays: J. M., X.W., and H.C. Ufd4-related western-blot assays: Q. Z. and J. M. TRIP12-related in vitro enzymatic assays: X.W. Identification the topology of polyubiquitin chains generated by Ufd4 on K48-linked diUb: J. M. and Q. Z. The manuscript writing: X. W., H. A., J. M., Z. D., Q. Z., L. Liu., and M. P. The project supervision: Q. Z., L. Liu., and M. P.

Competing interests Statement

The authors declare no competing interests.

Figure Legends/Captions

Figure 1. Ufd4 prefers to synthesize K29/K48-branched ubiquitin chains on K48-linked ubiquitin chains. a, Ufd4-dependent in vitro ubiquitination on fluorescent MonoUb and K48-linked diUb. Gel images and columns of relative conversions (%) are shown. Gel images are representative of independent biological replicates (n = 2). **b**, Schematic representation of the identification flow of Ub topology generated by Ufd4 on K48-linked Ub chains. The blue symbols represent the isopeptide bond between Lys48 and Ub C-terminal, the red symbols represent the isopeptide bond between Lys29 and Ub C-terminal, the grey symbols represent Ub C-terminals. **c**, Intact MS analysis of in vitro ubiquitination reactions treated with Lb^{pro}*, and the spectra were deconvoluted. Deconvoluted spectra (left), quantification of the relative abundance of each ubiquitin species (right) are shown. Data represent the mean ± SD of three independent experiments. **d**, Identification of K29/K48-branched ubiquitin chains. The MS/MS spectrum corresponding to the signature peptide derived from K29/K48-branched linkages (aa 29–57, GlyGly modified at K29 and K48) was obtained. **e,** Ufd4-dependent in vitro ubiquitination on fluorescent K48-linked diUb with lysine to arginine mutation at the proximal or distal Lys29 sites. Gel images are representative of independent biological replicates (*n* = 3). **f,** The Ufd4's ubiquitination activity on K48-linked triUb with a K29-only residue in the proximal, middle or distal Ub. Gel images are representative of independent biological replicates (*n* = 2). Source data are provided as a Source Data file.

Figure 2. Overall structure of Ufd4 in complex with $triUb^{K29/K48}$. a, Schematic of two-step complex assembly routes of Ufd4 in complex with $triUb^{K29/K48}$. Step one: synthetic route of the intermediate structure mimicking the transition state of Ufd4 mediated ubiquitination at proximal Lys29 site of K48-linked diUb. Step two: in vitro crosslinking experiments between Ufd4 and $triUb^{K29/K48}$. **b**, Schematic diagram of the native transition state *vs.* the transition state mimic of the ubiquitination process. The side chain of Lys29 residue on K48-linked diUb attacks the thioester bond of Ufd4–Ub. An intermediate structure design is shown in the inset to mimic the transition state of Ufd4-mediated Ub chain assembly. **c**, Structural domain diagram of Ufd4 with indicated residue boundaries. The dashed-line box indicates unresolved N-terminus region, the turquoise box represents the Ub binding

907 domains, the dusty blue box indicates the HECT domain and the red line represents the active Cys1450.
908 **d, e,** Cryo-EM density (**d**) and structural model (**e**) of the Ufd4-triUb$^{K29/K48}$ complex.

909

910 **Figure 3. Analysis of the interactions between Ufd4 and triUb$^{K29/K48}$. a,** Cryo-EM density of the
911 ARM region and the HECT C-lobe with K48-linked diUb, dashed regions correspond to interfaces
912 between Ufd4 and Ub$^{K48\text{-}dist}$, Ufd4 and Ub$^{K48\text{-}prox}$. **b-d**, Molecular interactions between the ARM region
913 and Ub$^{K48\text{-}dist}$ (**b**), the ARM region and Ub$^{K48\text{-}prox}$ (**c**), the HECT C-lobe and Ub$^{K48\text{-}prox}$ (**d**). **e,** Cryo-EM
914 density of the HECT C-lobe with donor Ub. **f,** Molecular interactions between the HECT C-lobe and
915 donor Ub. **g-h,** Cryo-EM density of the HECT C-lobe and triUb$^{K29/K48}$ (**g**), and the structural model
916 showing the spatial proximity of HECT C-lobe Cys1450, Lys29 of Ub K48-prox and C-terminal of
917 donor Ub (**h**). **i-j**, In vitro Ufd4-dependent ubiquitination assays. Mutants at the substrate recognition
918 interface (**i**) and the donor Ub interface (**j**) were tested. Gel images are representative of independent
919 biological replicates (n = 3). Source data are provided as a Source Data file.

920

921 **Figure 4. Analysis of the interactions between TRIP12 and triUb$^{K29/K48}$. a,** Cryo-EM density (**a**)
922 and structural model (**b**) of the TRIP12-triUb$^{K29/K48}$ complex. **c**, Structural alignment of Ufd4-
923 triUb$^{K29/K48}$ complex and TRIP12-triUb$^{K29/K48}$ complex structures, and only ARM region, C-lobe and
924 K48-linked diUb are shown. **d-e**, Molecular interactions between the ARM region and Ub$^{K48\text{-}dist}$ (**d**),
925 the ARM region and Ub$^{K48\text{-}prox}$ (**e**). **f-h**, Molecular interactions between the C-lobe and Ub$^{K48\text{-}prox}$.

926

927 **Figure 5. The structure of Ufd4 in complex with Ubc4-Ub. a,** Schematic of two-step complex
928 assembly routes of Ufd4 in complex with Ubc4-Ub. Step one: synthetic route of the intermediate
929 structure mimicking the transition state of Ufd4-mediated transthiolation from Ubc4-Ub. Step two: in
930 vitro crosslinking experiments between Ufd4 and Ubc4-Ub. **b**, Schematic diagram of the native
931 transition state vs. the transition state mimic of the transthiolation process. The side chain of catalytic
932 Cys residue on Ufd4 attacks the thioester bond of Ubc4–Ub. An intermediate structure design is shown
933 in the inset to mimic the transition state of the Ufd4-mediated transthiolation process. **c**, Cryo-EM
934 density and structural model of the Ufd4$^{\Delta ARM}$-Ubc4 complex. **d-g**, Molecular interactions between the
935 HECT C-lobe and Ubc4 (**d**), the HECT N-lobe and Ubc4 (**e-g**). **i-j**, In vitro Ufd4~Ub thioester
936 formation assays. Ubc4 mutants (**i**) and Ufd4 mutants (**j**) were tested. Gel images are representative of
937 independent biological replicates (n = 2). Source data are provided as a Source Data file.

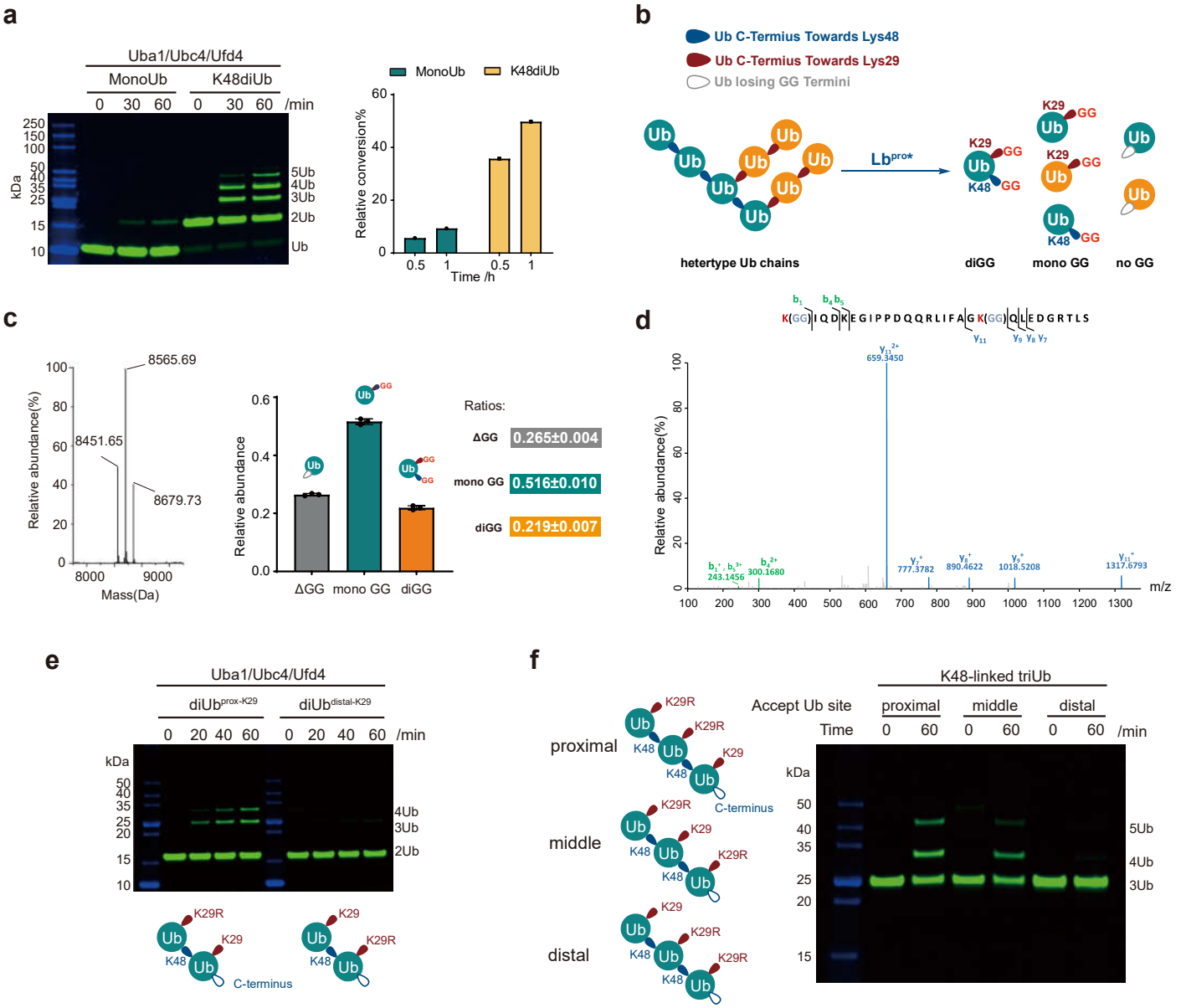
a
Uba1/Ubc4/Ufd4
MonoUb
K48diUb
0 30 60 0 30 60 /min
kDa
250
150
100
50
40
35
25
15
10
5Ub
4Ub
3Ub
2Ub
Ub
MonoUb
K48diUb
Relative conversion%
Time /h
b
Ub C-Termius Towards Lys48
Ub C-Termius Towards Lys29
Ub losing GG Termini
Lbpro*
hetertype Ub chains
diGG
mono GG
no GG
c
Relative abundance(%)
8565.69
8451.65
8679.73
Mass(Da)
Relative abundance
ΔGG
mono GG
diGG
Ratios:
ΔGG 0.265±0.004
mono GG 0.516±0.010
diGG 0.219±0.007
d
Relative abundance(%)
m/z
e
Uba1/Ubc4/Ufd4
diUbprox-K29
diUbdistal-K29
0 20 40 60 0 20 40 60 /min
kDa
4Ub
3Ub
2Ub
C-terminus
f
K48-linked triUb
Accept Ub site
proximal
middle
distal
Time 0 60 0 60 0 60 /min
kDa
5Ub
4Ub
3Ub
C-terminus

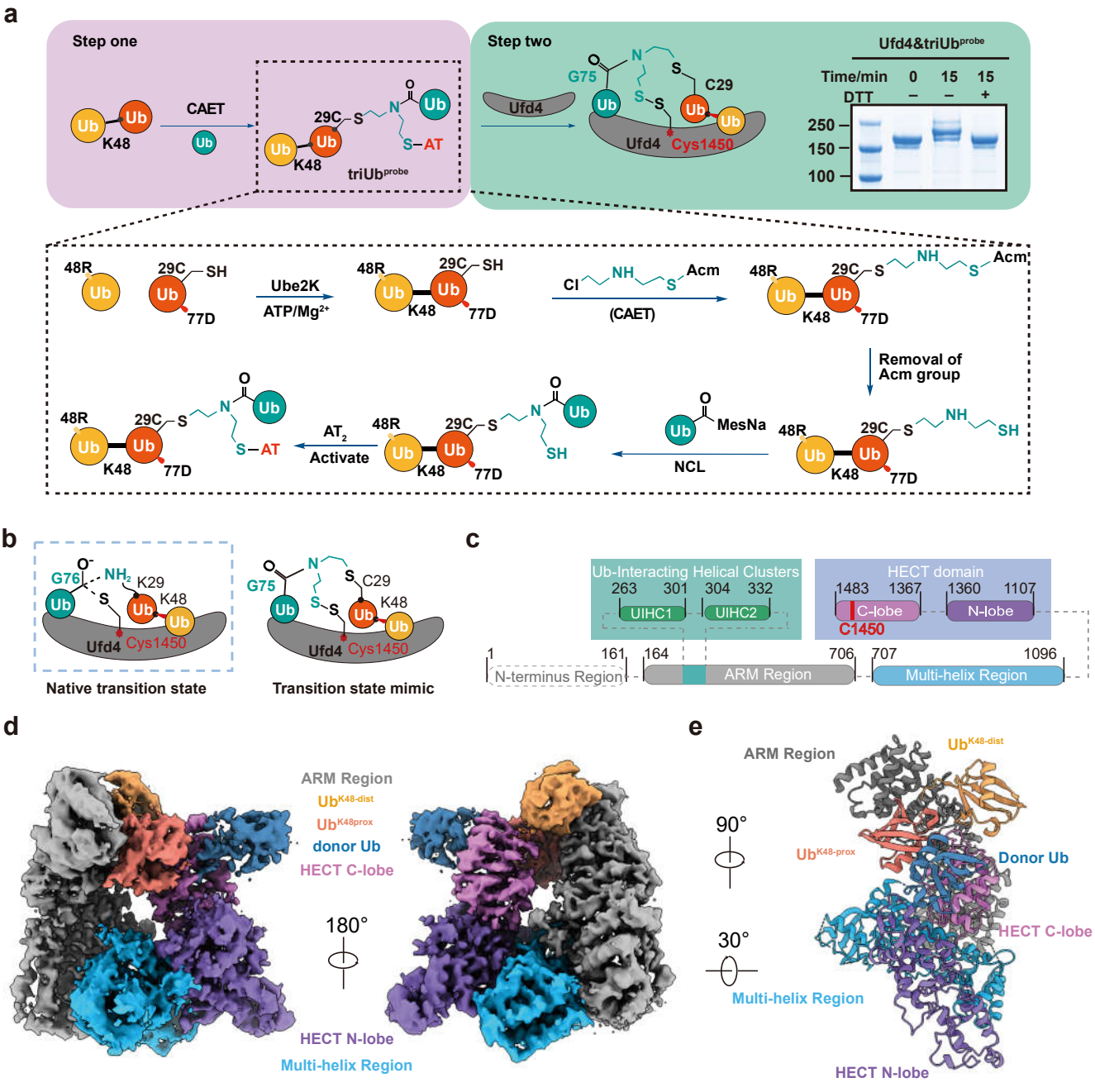
a
Step one
CAET
K48
triUb^probe
Step two
Ufd4
G75
C29
Cys1450
Ufd4&triUb^probe
Time/min 0 15 15
DTT – – +
250
150
100
Ube2K
ATP/Mg2+
(CAET)
Removal of Acm group
NCL
MesNa
AT2
Activate
77D
b
Native transition state
Transition state mimic
c
Ub-Interacting Helical Clusters
263 301 304 332
UIHC1
UIHC2
HECT domain
1483 1367 1360 1107
C-lobe
N-lobe
C1450
1 161 164 706 707 1096
N-terminus Region
ARM Region
Multi-helix Region
d
ARM Region
Ub^K48-dist
Ub^K48prox
donor Ub
HECT C-lobe
180°
HECT N-lobe
Multi-helix Region
e
ARM Region
Ub^K48-dist
90°
Ub^K48-prox
Donor Ub
HECT C-lobe
30°
Multi-helix Region
HECT N-lobe

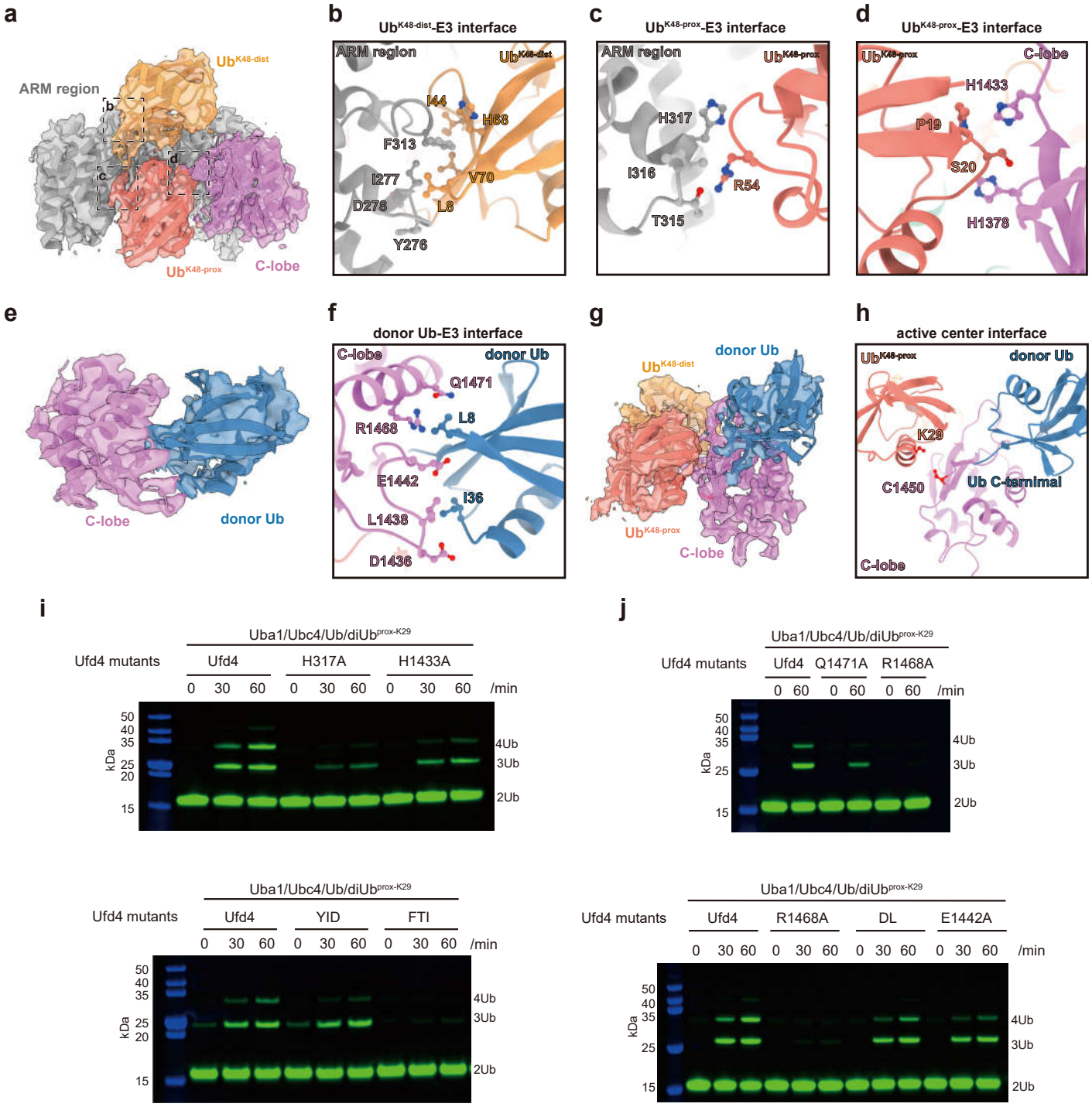
a
ARM region
Ub K48-dist
Ub K48-prox
C-lobe
b
c
d
b
Ub K48-dist-E3 interface
ARM region
Ub K48-dist
I44
H68
F313
I277
V70
D278
L8
Y276
c
Ub K48-prox-E3 interface
ARM region
Ub K48-prox
H317
I316
R54
T315
d
Ub K48-prox-E3 interface
Ub K48-prox
C-lobe
H1433
P19
S20
H1378
e
C-lobe
donor Ub
f
donor Ub-E3 interface
C-lobe
donor Ub
Q1471
L8
R1468
E1442
I36
L1438
D1436
g
donor Ub
Ub K48-dist
Ub K48-prox
C-lobe
h
active center interface
Ub K48-prox
donor Ub
K29
C1450
Ub C-terminal
C-lobe
i
Uba1/Ubc4/Ub/diUb prox-K29
Ufd4 mutants
Ufd4
H317A
H1433A
0 30 60 0 30 60 0 30 60 /min
kDa
50
40
35
25
20
15
4Ub
3Ub
2Ub
Uba1/Ubc4/Ub/diUb prox-K29
Ufd4 mutants
Ufd4
YID
FTI
0 30 60 0 30 60 0 30 60 /min
kDa
50
40
35
25
20
15
4Ub
3Ub
2Ub
j
Uba1/Ubc4/Ub/diUb prox-K29
Ufd4 mutants
Ufd4
Q1471A
R1468A
0 60 0 60 0 60 /min
kDa
50
40
35
25
15
4Ub
3Ub
2Ub
Uba1/Ubc4/Ub/diUb prox-K29
Ufd4 mutants
Ufd4
R1468A
DL
E1442A
0 30 60 0 30 60 0 30 60 0 30 60 /min
kDa
50
40
35
25
15
4Ub
3Ub
2Ub

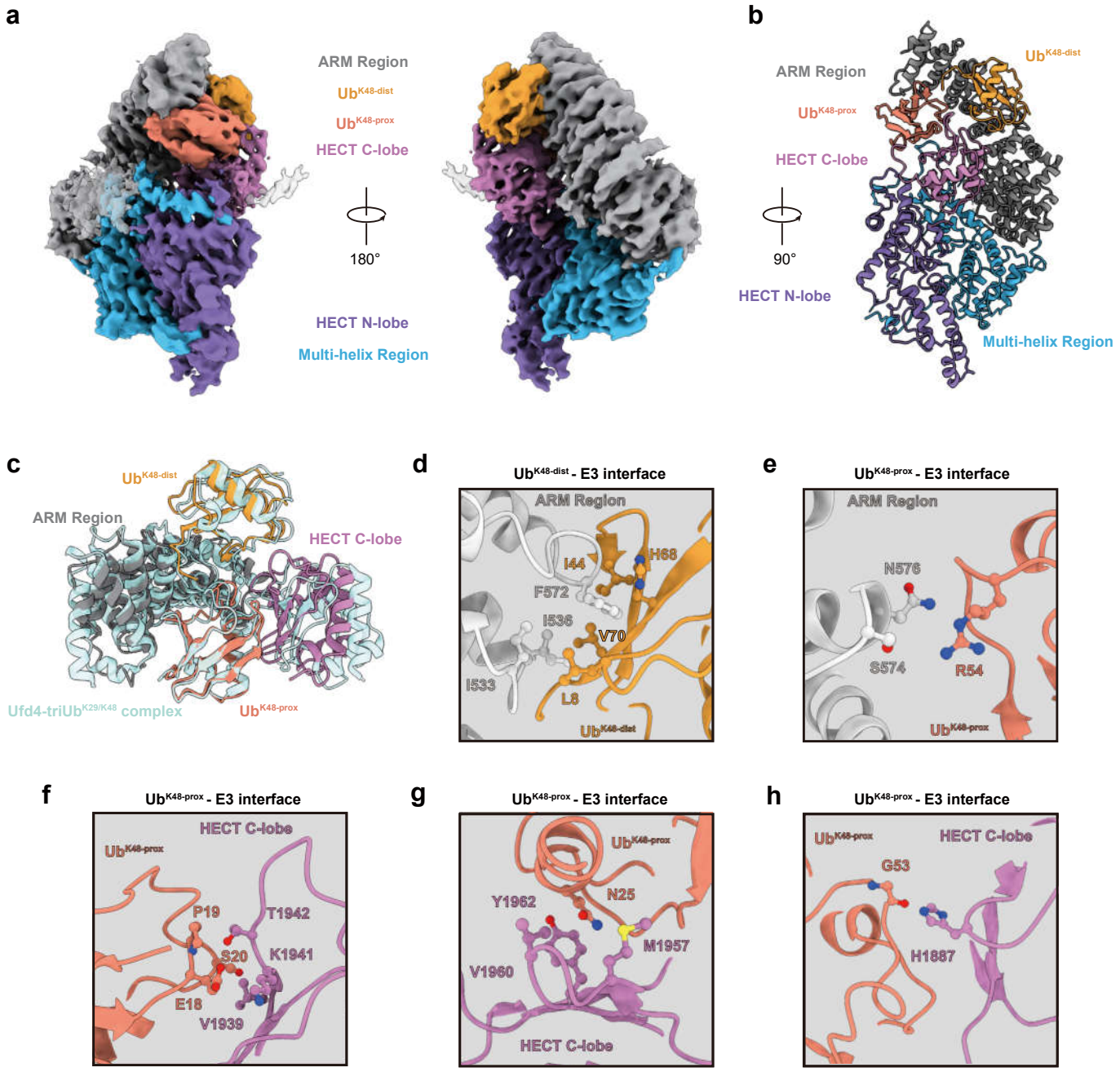
a
ARM Region
UbK48-dist
UbK48-prox
HECT C-lobe
180°
HECT N-lobe
Multi-helix Region
b
ARM Region
UbK48-dist
UbK48-prox
HECT C-lobe
90°
HECT N-lobe
Multi-helix Region
c
UbK48-dist
ARM Region
HECT C-lobe
Ufd4-triUbK29/K48 complex
UbK48-prox
d
UbK48-dist - E3 interface
ARM Region
I44
H68
F572
I536
V70
I533
L8
UbK48-dist
e
UbK48-prox - E3 interface
ARM Region
N576
S574
R54
UbK48-prox
f
UbK48-prox - E3 interface
HECT C-lobe
UbK48-prox
P19
T1942
S20
K1941
E18
V1939
g
UbK48-prox - E3 interface
UbK48-prox
Y1962
N25
M1957
V1960
HECT C-lobe
h
UbK48-prox - E3 interface
UbK48-prox
HECT C-lobe
G53
H1887

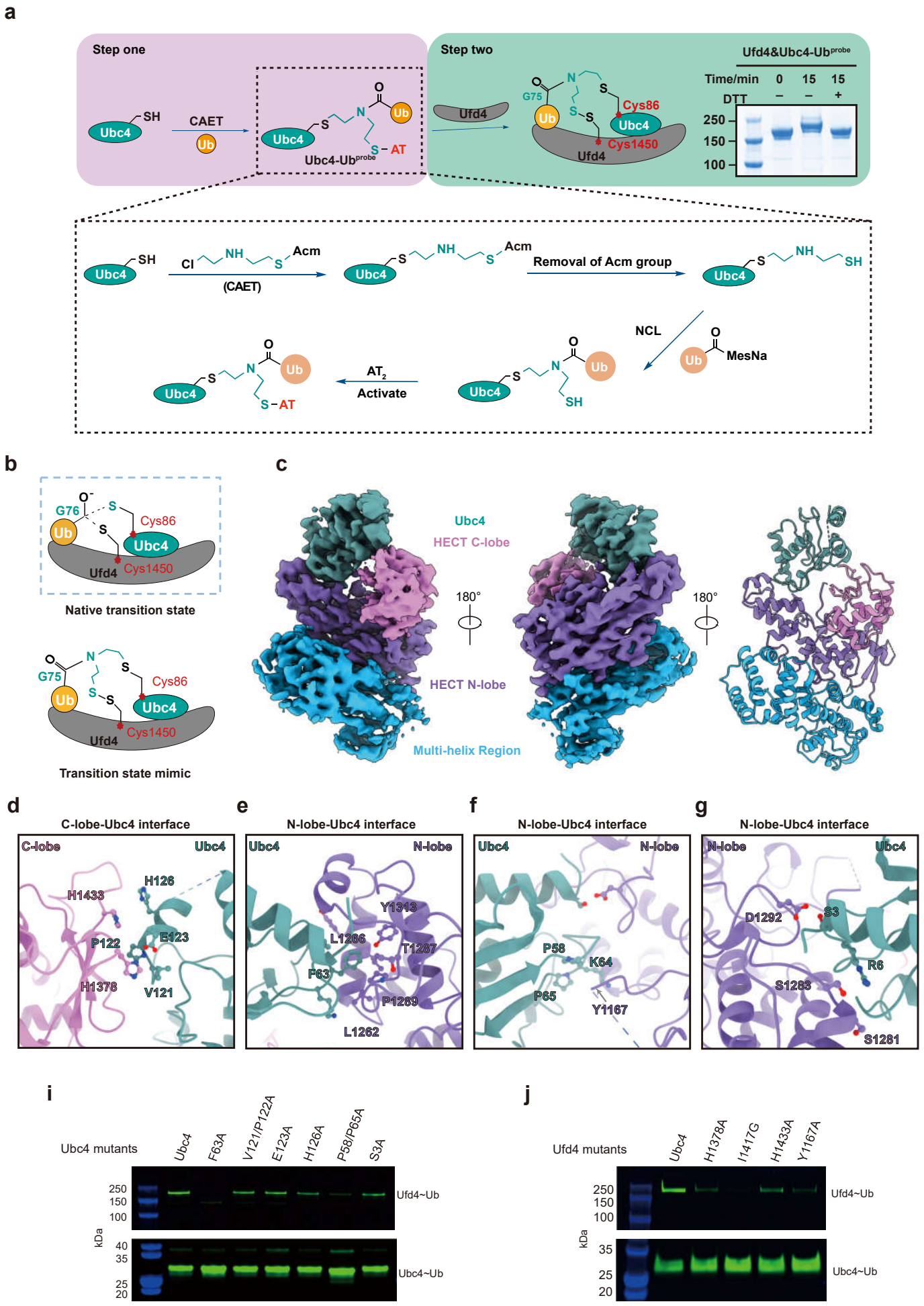
a
Step one
Ubc4
SH
CAET
Ub
Ubc4-Ub^probe
AT
Step two
Ufd4
G75
Cys86
Cys1450
Ufd4&Ubc4-Ub^probe
Time/min 0 15 15
DTT – – +
250
150
100
Acm
(CAET)
Removal of Acm group
NCL
MesNa
AT2
Activate
b
Native transition state
Transition state mimic
c
Ubc4
HECT C-lobe
HECT N-lobe
Multi-helix Region
180°
d
C-lobe-Ubc4 interface
C-lobe
H126
H1433
P122
E123
H1378
V121
e
N-lobe-Ubc4 interface
N-lobe
Y1313
L1266
T1287
F63
P1269
L1262
f
N-lobe-Ubc4 interface
P58
K64
P65
Y1167
g
N-lobe-Ubc4 interface
D1292
S3
R6
S1283
S1281
i
Ubc4 mutants
Ubc4
F63A
V121/P122A
E123A
H126A
P58/P65A
S3A
Ufd4~Ub
Ubc4~Ub
kDa
250
150
100
40
35
25
20
j
Ufd4 mutants
Ubc4
H1378A
I1417G
H1433A
Y1167A
Ufd4~Ub
Ubc4~Ub
kDa
250
150
100
35
25
20